International Journal of Heat and Mass Transfer 156 (2020) 119854

Contents lists available at ScienceDirect

International Journal of Heat and Mass Transfer

journal homepage: www.elsevier.com/locate/hmt

Mechanistic method to predicting minimum heat flux point wall temperature in saturated pool boiling

Chang Cai[a,b], Issam Mudawar[b,*], Hong Liu[a]

[a] Key Laboratory of Ocean Energy Utilization and Energy Conservation of Ministry of Education, School of Energy and Power Engineering, Dalian University of Technology, Dalian, 116024, PR China

[b] Purdue University Boiling and Two-Phase Flow Laboratory (PU-BTPFL), School of Mechanical Engineering, 585 Purdue Mall, West Lafayette, IN 47907, USA

ARTICLE INFO

Article history:
Received 24 January 2020
Revised 21 April 2020
Accepted 22 April 2020
Available online 18 May 2020

Keywords:
Minimum heat flux point
Pool boiling
Interfacial instability
Minimum film boiling temperature

ABSTRACT

This study details the development of a new mechanistic approach to predicting heating wall temperature corresponding to the minimum heat flux (MHF) point for saturated pool boiling from a horizontal flat surface. The model is constructed by performing a force balance on a unit cell of the wavy liquid-vapor interface, incorporating the effects of pressure difference across the interface, surface tension, gravity and stagnation pressure. It is shown how, in the film boiling regime, where a continuous vapor film insulates the heating surface, a decrease in wall heat flux towards the MHF point causes the liquid to approach the surface but without yielding any contact. A further decrease in heat flux triggers the MHF condition once the downward forces pushing the interface towards the wall overcome the upward forces lifting the interface away from the wall. This causes the wavy liquid-vapor interface to contact and wet the heating surface; vigorous bubble nucleation and vapor production ensue, signaling onset of the transition boiling regime. To achieve closure, the model adopts a previous relation for film boiling heat transfer coefficient, which is used to determine the wall temperature . The new model is shown to provide good agreement with MHF-point wall temperature data for many liquids and a broad range of pressures, evidenced by a mean absolute error of 9.35%. This study also includes an assessment of previous thermodynamic and hydrodynamic MHF models.

1. Introduction

1.1. Phase change thermal management schemes

Phase change processes are prevalent in many traditional and modern industrial applications. The former includes steam power generation, refrigeration and air conditioning, food processing, pharmaceuticals, and materials processing [1]; this is where predictable and reliable system operation is highly dependent on the ability to predict both dominant interfacial behavior and corresponding heat transfer performance. As to modern applications, most involve the need to dissipate large amounts of heat per area while maintaining relatively low surface temperatures; they include computer electronics, data centers, hybrid vehicle power electronics, aircraft and spacecraft avionics, and x-ray medical devices, to name a few [1-3].

Much of the emphasis on phase change schemes is the outcome of their effectiveness at dissipating large amounts of heat, via both sensible and latent heat content of the cooling fluid. Realizing the benefits of phase change processes has been a primary focus of research efforts at Purdue University Boiling and Two-Phase Flow Laboratory (PU-BTPFL) spanning over three decades. These efforts encompass a variety of schemes, including heat pipes [4], pool boiling [5], falling film [6], macro-channel flow [7, 8], mini/micro-channel flow [9], jet impingement [10] and spray [11], as well as hybrid methods combining the merits of different schemes [12]. In these studies, three different approaches have been adopted to predict the heat transfer characteristics: (1) experimental, and through development of empirical correlations (*e.g.*, [13, 14]), (2) computational (*e.g.*, [15]), and (3) theoretical (*e.g.*, [16]).

Pool boiling, achieved by immersing a heat-dissipating surface in a stagnant pool of liquid coolant, is highly favored in many applications because of its relative simplicity and low cost. An important example of pool boiling that is closely related to the topic of the present study is bath quenching of metal parts in water, oils, molten salt and polymer solutions.

* Corresponding author.
E-mail address: mudawar@ecn.purdue.edu (I. Mudawar).
URL: https://engineering.purdue.edu/BTPFL (I. Mudawar)

https://doi.org/10.1016/j.ijheatmasstransfer.2020.119854
0017-9310/

Nomenclature

A	parameter defined in Table 1
A_t	atomic number
A_{tc}	transient contact area in Table 2
A_v	Avogadro number in Table 2
a	parameter defined in Table 2
a_1, a_2	coefficients in cavity size distribution in Table 2
B	parameter defined in Table 1
b	parameter defined in Table 2
C	constant in Table 1
CHF	critical heat flux
c	wave speed
c_p	constant-pressure specific heat
D	'minimum length' of heating surface
D'	ratio of surface area to perimeter
d	bubble diameter in Table 2
F	parameter defined in Table 2
F_P	pressure difference force
F_G	gravity force
F_S	stagnant pressure force
F_σ	surface tension force
f	bubble departure frequency in Table 2
f_1, f_2	parameters defined in Table 3
Ga	Galileo number
g	gravity
g_c	gravitational constant
h	heat transfer coefficient; enthalpy
h_{fg}	latent heat of vaporization
h_{fg}'	modified latent heat of vaporization in Table 3
J	nucleation rate
K	parameter defined in Eq. (20)
k	heat conductivity coefficient; wave number
LFP	Leidenfrost point
M	molar mass
MAE	maximum absolute error
MHF	minimum heat flux
m_1, m_2	parameters defined in Eq. (19)
Nu	Nusselt number
n	number of data points
$\|P\|$	parachor in Table 2
P	pressure
P_R	reduced pressure
Pr	Prandtl number
Q_a	heat of adsorption
q''	heat flux
Ra	Rayleigh number
R_g	gas constant
R_q	root mean square of surface roughness
R_z	average height of surface roughness
r	surface cavity radius in Table 2
S	arc length
T	temperature
T_{MS}	maximum superheat temperature
T_{min}	minimum film boiling temperature
T_{sat}	saturation temperature
ΔT_{min}	T_{min} - T_{sat}
t	time
$U_{g,n}$	vapor velocity normal to surface
V	molecular volume
v	specific volume
W	heater width
X	parameter defined in Table 1
z	coordinate parallel to free interface

Greek symbols

Λ	surface monolayer coverage fraction
α	thermal diffusivity; contact angle
β	parameter defined in Table 1
β_T	coefficient of cubical expansion in Table 3
χ	parameter defined in Eq. (14)
δ	vapor film thickness
ε	evaporation coefficient in Table 2
η	interfacial displacement
η_0	wave amplitude
Γ_0	number of adsorbed molecules per unit area to form a monolayer
λ	wavelength
λ_c	critical Taylor wavelength
μ	viscosity
Ω	percent liquid-solid interface coverage by vapor in Table 2
ρ	density
σ	surface tension
τ_0	residence time of molecule in the adsorbed state
θ	inclination angle
ξ	parameter defined in Table 2

Subscripts

B	based on Berenson's model
c	critical point
co	zero contact angle
exp	experiment (measured)
f	liquid
g	vapor
i	interface; imaginary component
max	maximum
min	minimum (corresponding to MHF point)
n	normal
pred	predicted
r	real component
sat	saturation
sub	subcooling
sup	superheated in Table 2
tp	triple point
w	wall (heating surface)

1.2. Pool boiling Minimum Heat Flux (MHF) point

In metal heat treating, great emphasis is placed on post-critical heat transfer characteristics, which include critical heat flux (CHF) and minimum heat flux (MHF) (or Leidenfrost point (LFP)) [17]. A great amount of work has been focused on experimental investigation, numerical modeling, and theoretical analysis of pool boiling CHF, which separates the transition and nucleate boiling regimes. Summaries of dominant CHF mechanisms and assessments of related models and correlations are available from recent reviews [18, 19]. On the contrary, there has been far less emphasis on MHF or LFP.

While both MHF and LFP correspond to the minimum film boiling temperature, T_{min}, and demarcate the film and transition boiling regimes, the former is encountered in pool boiling and the later discrete droplets. A number of other terms have also been used interchangeably to describe the same phenomena (although they may not be exactly synonymous). They include film boiling/vapor film collapse point, quenching point, rewetting point, foam limit, departure from film boiling, lower limit of stable film boiling (for situations involving decreasing surface temperature), and incipience of stable film boiling (for increasing surface temperature). The present study is focused entirely on minimum temperature corre-

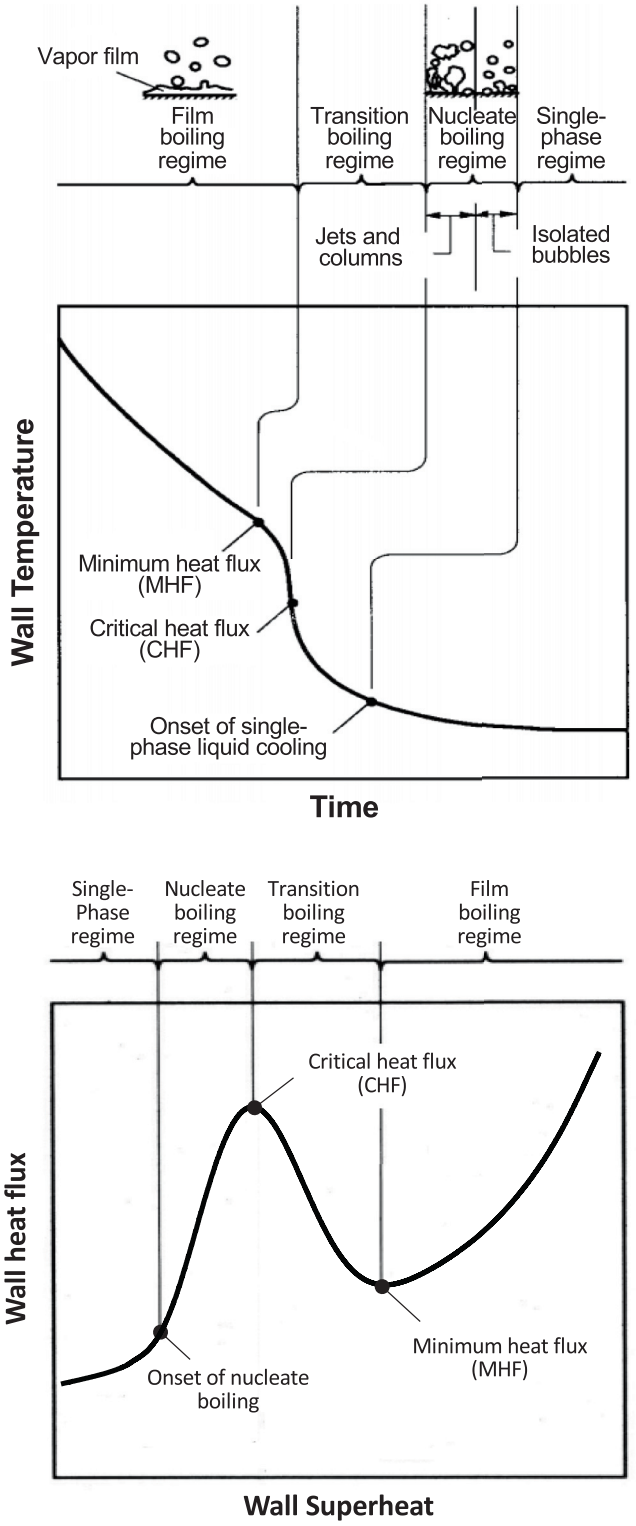

Fig. 1. Pool boiling curve and quench curve Fig. 2.

sponding to film pool boiling, for which MHF will be used exclusively.

As shown in Fig. 1, pool boiling MHF point is identified with the aid of either the quenching curve (wall temperature versus time), or the boiling curve (wall heat flux versus wall superheat). In laboratory experiments, transient quenching enables rapid capture of the complete quenching curve. Here, MHF marks the termination of the slow film boiling regime and onset of transition boiling. But this point is more discernable with the aid of the boiling curve, which is commonly measured using heat-flux-controlled experiments. Substantial changes in the relationship between heat flux and wall superheat above versus below the MHF point temperature reflect fundamental differences in hydrodynamic and thermal characteristics between film boiling and transition boiling. In the former, an insulating vapor film having very low thermal conductivity fully covers the wall, resulting in very poor heat transfer performance. Decreasing the heat flux to the MHF point causes partial collapse of the vapor film, which induces appreciable enhancement in heat transfer with commencement of the transition boiling regime.

The MHF point is of paramount importance to metal alloy heat treatment processes. These processes involve preheating the alloy part to a high temperature approaching the melting point, causing hardening compounds to dissolve fully into the primary metal crystals. This is followed by fast quenching of the part to near room temperature in an effort to preserve the solution. Subsequently, the part is heated to an intermediate temperature (between preheating and room temperatures) to allow the hardening compounds to coalesce into a fine dispersion within the primary metal crystals, which is how the alloy achieves desired improvements in both strength and hardness. The importance of the quench phase of heat treating can be explained as follows. Preserving the solution requires the quench proceed at an infinitely fast rate, which is impossible given the finite values of both the heat transfer coefficient and thermal mass of the part. Therefore, heat treating operations aim to simply accelerate the quench rate. Recall that the initial preheating is associated with high wall temperatures well within the film boiling regime, where the cooling rate is quite slow. Because the MHF point marks the instant cooling rate begins to accelerate, any means to achieve earlier occurrence of this event would contribute to a faster overall quench rate and therefore better mechanical properties. This explains two main needs in the heat-treating industry: (1) Accurate prediction of the MHF point, and (2) methods for accelerating MHF occurrence; the present study concerns the former.

1.3. Experimental studies on pool boiling MHF point

Experimental study of pool boiling MHF point has been the focus of numerous studies. Table 1 provides a summary of these studies specific to boiling from flat horizontal surfaces. As can be seen from this table, MHF point is influenced by many parameters, including those associated with the boiling fluid (*e.g.,* pressure, degree of liquid subcooling, liquid depth, and thermophysical properties) as well as the boiling surface (*e.g.,* shape and size, material properties, roughness, oxidation, porosity, and wettability). Ignoring one or more of these influences may explain the considerable scatter when comparing data from different sources. Despite this scatter, there is general agreement that increases in liquid subcooling and/or system pressure significantly increase both the heat flux, q''_{min}, and wall temperature, T_{min}, corresponding to the MHF point.

Also included in Table 1 are empirical correlations for key pool boiling MHF point parameters. Although these correlations provide satisfactory predictions of heat flux and/or wall temperature, their validity is limited to only the ranges of parameters specific to each correlation. Additionally, most correlations ignore the influences of secondary parameters, especially ones associated with surface condition.

The fluids used in previous MHF point experiments can be categorized into three types (based mostly on practical use): (1) Normal fluids like water and organic liquids, which are encountered in numerous boiling applications at or near atmospheric pressure, (2)

Table 1
Summary of experimental studies on pool boiling MHF point temperature/heat flux.

Author(s)	Fluid(s)	Subcooling	System pressure	Surface characteristics	Main conclusions/Correlations
	Horizontal flat surface				
Berenson [20] (1962)	n-pentane, CCl_4	0	0.1 MPa	Inconel, copper and nickel (mirror finish, milled, slightly oxidized and oxidized), D = 50.8 mm	MHF and T_{min} are independent of surface material and roughness for contact angles of commercial importance
Hosler & Westwater [21] (1962)	water, CCl_3F	-	0.1 MPa	Aluminum (polished), 203.2 × 203.2 mm	MHF is caused by Taylor hydrodynamic instability. MHF and T_{min} are 3.47 W/cm^2 and 414 K for water, and 1.80 W/cm^2 and 344 K for CCl_3F.
Cummings & Smith [22] (1966)	liquid helium	-	0.1 MPa	Copper (various roughnesses), D = 15.24 mm	MHF increases by a factor of 15 as the thickness of the H_2O crystal coating increases up to about 1 mm.
Padilla [23] (1966)	potassium	0-10	0.267-40 kPa	Stainless steel, D = 76.2 mm	MHF = 0.63 W/cm^2, T_{min} = 865.5 K @ 0.267 kPa, MHF = 2.84 W/cm^2, T_{min} = 1063.5 K @ 6.67 kPa. $MHF = 0.14\rho_g h_{fg}[\frac{\sigma g(\rho_f-\rho_g)}{(\rho_f+\rho_g)^2}]^{1/4}$
Clark et. al. [24] (1967)	liquid nitrogen	0	0.1 MPa	Copper, D = 76.2 mm	MHF = 1.525 W/cm^2, ΔT_{min} = 34.3 K.
Kesselring *et al.* [25] (1967)	R113	0	0.1 MPa	Stainless steel (various widths)	MHF depends on strip width for small widths less than $2\lambda_d$. $MHF = \frac{0.1612\pi}{3^{5/4}}\frac{\rho_g h_{fg}\sigma g(\rho_f-\rho_g)}{(\rho_f+\rho_g)^2}$
Butler *et al.* [26] (1970)	liquid helium	-	-	Copper (roughened, coated, frosted), 50 × 10 mm	Roughening has a small effect on MHF, while a thin insulating layer has a marked effect. MHF increases by a factor of up to about 4 compared to a smooth copper surface.
Tachibana & Enya [27] (1973)	R113, ethanol, water, oil	0-30	-	Copper, D = 18, 50 mm	MHF increases significantly with increasing subooling.
Swanson *et al.* [28] (1975)	liquid nitrogen	0	0.1 MPa	Sapphire (polished), D = 12.7 mm	MHF = 6.56 W/cm^2, ΔT_{min} = 29.5 K.
Deev *et al.* [29] (1977)	liquid helium	-	$0.445<P_R<0.98$	Copper (polished, R_z = 0.08 μm), 30 × 30 mm	MHF and ΔT_{min} decrease with increased P_R.
Peyayopanakul & Westwater [30] (1978)	liquid nitrogen	-	0.1 MPa	Copper, D = 50.8 mm	MHF varies from 0.1-0.9 W/cm^2, but T_{min} is approximately constant at 20 K.
Ibrahim [31] (1978)	liquid helium	0-2.5	0.036-0.197 MPa	Copper, D = 25.4 mm	Subcooling increases MHF appreciably. MHF = 0.31 W/cm^2 @ 0.97 atm.
Yao & Henry [32] (1978)	ethanol, water	0	<1.5 MPa	Stainless steel and copper (with and without gold layer)	T_{min} is determined either by a Taylor instability vapor removal limitation or by spontaneous nucleation upon contact.
Kobayashi & Yasukōchi [33] (1980)	liquid helium	-	-	Nichrome, 6.4 mm^2	MHF increases and then decreases with increasing liquid temperature, and increases with increased immersion depth.
Scheiwe & Hartmann [34] (1982)	liquid nitrogen	-	-	Copper (R_z = 0.75, 12.6 μm), 264 cm^2	MHF = 0.6 W/cm^2, ΔT_{min} = 22.7 K.
Dhuga & Winterton [35] (1985)	water, methanol	0	0.1 MPa	Aluminum (anodized)	MHF and ΔT_{min} are, respectively, 2.76-4.15 W/cm^2 and 68-75 K for methanol, and 16.14-18.71 W/cm^2 and 201-212 K for water.
Jung *et al.* [36] (1987)	R11	0.5-1	-	Copper (polished, R_q = 1.56 μm), steel (particle coated, R_q = 6.61, 11.7 μm), D = 78 mm	MHF and T_{min} increase with increasing pressure, and surface treatment causing higher roughness and porosity significantly increases T_{min}.
Shoji & Nagano [37] (1987)	R113	0	0.05-0.90 MPa	Copper, D = 62 mm	$MHF = 0.00189\rho_g h_{fg}(\frac{\rho_g}{\rho_f})^{-0.73}[\frac{\sigma g(\rho_f-\rho_g)}{(\rho_f+\rho_g)^2}]^{1/4}\frac{\rho_g}{\rho_f} > 5\times10^{-3}$ $MHF = 0.0212\rho_g h_{fg}(\frac{\rho_g}{\rho_f})^{-0.26}[\frac{\sigma g(\rho_f-\rho_g)}{(\rho_f+\rho_g)^2}]^{1/4}\frac{\rho_g}{\rho_f} < 5\times10^{-3}$
Shoji *et al.* [38] (1987)	water	0	0.1 MPa	Copper, D = 10-150 mm	End effects on MHF can be eliminated with surface size larger than $3\lambda_d$.
Ramilison & Lienhard [39] (1987)	R113, acetone, benzene, n-pentane	0	0.1 MPa	Copper (roughened, mirror-polished, Teflon-coated), D = 63.5 mm	Vapor film collapse occurs as the extent of surface contact increases, which is indicated by the advancing contact angle.
Nishio & Chandratillek [40] (1989)	liquid helium	0	0.1 MPa	Copper (R_a = 0.027, 0.06, 0.46, 1.27, 4.35 μm), D = 20 mm	T_{min} is affected by neither surface roughness nor orientation; $\Delta T_{min} \approx$ 2 K.
Abbassi *et al.* [41] (1989)	water, methanol	0	0.1 MPa	Aluminum (anodized), D = 15.5-26.0 mm	MHF and T_{min} for a confined surface are independent of surface diameter in a range comparable with λ_d.
Westwater *et al.* [42] (1989)	R116, ethane	-	0.1 MPa	Copper (polished), D = 50 mm	For R116: MHF = 1.8 W/cm^2, ΔT_{min} = 40 K. For ethane: MHF = 2.2 W/cm^2, ΔT_{min} = 48 K.

(*continued on next page*)

Table 1 (*continued*)

Author(s)	Fluid(s)	Subcooling	System pressure	Surface characteristics
Shoji et. al. [43] (1990)	water	0	0.1 MPa	Copper (polished, oxidized, R_a = 0.045, 0.097, 0.0500, 0.174 μm), D = 100 mm
Rajab & Winterton [44] (1990)	water, R113	0	0.1 MPa	Aluminum and copper (polished, anodized), D = 27 mm
Chang *et al.* [45] (1998)	FC-72, FC-87	0	0.1 MPa	Copper (polished, microporous coated), 10 × 10 mm
Takata *et al.* [46] (2005)	water	0	-	Copper (bare and coated with TiO_2), D = 17 mm
Ahn *et al.* [47, 48] (2009)	PF-5060	0-30	0.1 MPa	Silicon (bare, coated with nanotubes of different heights), 58.74 × 31.75 mm
Zhao *et al.* [49] (2014)	R14	0	0.1 MPa	Copper (R_z = 57.3 nm, R_a = 46.7 nm), D = 20 mm
Li *et al.* [50] (2018)	liquid nitrogen	-	0.1 MPa	Copper, sandstone (polished, sand coated, grooved, oil-covered), D = 80 mm
Other surface configuration				
Baumeister & Simon [51] (1973)	Various liquid types (using previous data for cryogens, water, liquid metals, and hydrocarbons)	0	-	Smooth clean surfaces (using previous data for both droplet and pool on flat surfaces, spheres and cylinders)
Nishio [52] (1987)	Various liquid types (using previous data and the author's own data for water, liquid nitrogen)	0	0.1 MPa	Smooth surfaces (using previous data for flat surfaces, spheres and cylinders, and the author's own data for horizontal cylinders)
Klimenko & Snytin [53] (1990)	Various liquid types (using previous data and the authors' own data for water, liquid nitrogen)	Various subcooling	Various pressures	Smooth surfaces (using previous data for flat surfaces, spheres and cylinders, and the authors' own data for spheres)
Other empirical correlations				
Kalinin *et al.* [54] (1975)				$T_{min} = T_{sat} + (T_c - T_{sat})[0.16 + 2.4(\frac{k_f \rho_f c_{pf}}{k_w \rho_w c_{pw}})^{1/4}]$, $q''_{min} = 0.18\Delta T_{min}[\frac{c_{pg} k_g^2}{\mu_g} \rho_g g(\rho_f - \rho_g)]^{1/3}$
Morozov* (1962)				$q''_{min} = 0.206\rho_g h_{fg}\sigma[\frac{g\rho_g(\rho_f - \rho_g)}{\mu_g^2}]^{0.4}[\frac{\sigma}{g(\rho_f - \rho_g)}]^{0.1}$
Nikolayev & Skripov* (1970)				Low-pressure region: $q''_{min} = 1.67 q''_{min}{}^{*}(P/P_c)^{0.24}(1 - P/P_c)^{0.61}$, where $q''_{min}{}^{*} = q''_{min}\|_{P^*=0.31P_c}$. Near-critical pressure region: $q''_{min} = 4.18 q''_{min}{}^{*}(P/P_c)^{0.24}(1 - P/P_c)^{0.61}$, where $q''_{min}{}^{*} = q''_{min}\|_{P^*=0.90P_c}$
Berlin *et al.** (1986)				$\frac{T_{min} - T_{sat}}{T_c - T_{sat}} = [0.16 + 2.5(\frac{k_f \rho_f c_{pf}}{k_w \rho_w c_{pw}})^{1/4} + \frac{k_f \rho_f c_{pf}}{k_w \rho_w c_{pw}}](1 + 0.13\cos\theta)\frac{1+\cos\alpha}{2}$ for $(k\rho c_p)_f/(k\rho c_p)_w = 10^{-6} - 1$, θ = 0-180°, $\alpha \leq 50°$, $D > 5[g(\rho_f - \rho_g)/\sigma]^{-1/2}$ and $P/P_{cr} = 0.005 - 0.63$

* As referenced by Klimenko & Snytin [53] (1990)

liquid metals, important to high temperature and pressure space and nuclear power applications, and (3) cryogenic fluids, like helium and nitrogen, which correspond to very low operating temperatures. Overall, it is important to be mindful of the fundamental differences in thermal-hydraulic characteristics among the three fluid types.

A key concern when using published MHF data is that many authors ignore the effects of secondary parameters, especially surface condition, which compromises the accuracy of any correlations based on individual databases. This issue clearly requires further investigation and points to the need to conduct future experiments under broad yet highly controlled conditions, accounting for all the above-mentioned fluid and surface parameters.

1.4. Theoretical prediction of pool boiling MHF point

While pool film boiling has been the subject of numerous theoretical studies, because of limited understanding of the MHF point, modeling attempts for MHF are quite sparse. Available theoretical works related to pool boiling MHF point for flat horizontal surfaces are summarized in Table 2. It shows all prior works are based on one of two types of mechanistic treatments: *thermodynamic* and *hydrodynamic*. The *thermodynamic* models are based on the premise liquid-solid contact will occur when the interfacial fluid/surface temperature falls below the liquid's maximum superheat temperature, T_{MS}. Different methods have been adopted to determine this temperature, including the equation of state, homogeneous/heterogenous nucleation theory, and wettability hypotheses. And, a few simple formulations for T_{MS} have also been proposed as a function of the critical temperature alone. Overall, the *thermodynamic* models ignore altogether surface effects as well as the influence of many important fluid properties; they also fail to account for the important effects of interfacial hydrodynamics. These models therefore serve mostly as first order approximations for the MHF point wall temperature.

On the other hand, the more popular *hydrodynamic* models are based on a combination of bubble dynamics and interface instability theory. As will be discussed later, interactions between flow momentum of individual phases, body force, and surface tension force are known to trigger instabilities along liquid-vapor interface, which, in turn, have profound influences on both heat and mass transfer during boiling. One of the earliest theoretical and mechanistic hydrodynamic models for MHF on a horizontal surface is proposed by Zuber [55], who incorporated the Rayleigh-Taylor instability to describe the shape of the vapor-liquid interface. He postulated that MHF depends on bubble release frequency, energy transport to the vapor bubble, and heater area producing a single bubble. As indicated in Table 2, several subsequent pool boiling MHF models are perturbations to Zuber's original treatment, which is evidenced by most of these models having the same functional form as Zuber's, except for using a different empirical multiplier.

Another very popular theoretical model for MHF is one proposed by Berenson [56], who incorporated the Taylor-Helmholtz instability theory and suggested a correction to the coefficient in Zuber's model to improve the predictive accuracy. Berenson's model relies on a semi-analytical expression for the film boiling heat transfer coefficient to obtain the MHF wall temperature. Although this model showed ±10% agreement with Berenson's own data [20], expressions for key parameters in the model were derived from measurements corresponding to narrow ranges of experimental conditions. These include such empirical information as bubble radius and average bubble height above the vapor film.

Later, Henry [57] showed that the Berenson's model predicts wall temperatures lower than those measured. To improve predictions, Henry incorporated the effects of thermal properties (product $k\rho c_p$) of both liquid and solid wall into the Berenson's model. He proposed that transient surface wetting induces local depression in the wall temperature, resulting in the vapor film collapsing at a higher wall temperature. Despite these improvements, his model, like Berenson's, employed parameters obtained from measurements corresponding to limited ranges of operating conditions. This compromises the validity of the model beyond these conditions.

Gunnerson and Croenenberg [58, 59] extended Zuber's model to film boiling on spherical surfaces. Afterwards, they extended their model to film boiling on a flat surface by assuming that the vapor removal mechanism from the latter is similar to that from a spherical surface for sphere diameters ten times or greater than the critical Taylor wavelength. Their model incorporates the effects of transient liquid-solid contact, interfacial wettability, and liquid subcooling, but also includes empirical correlations for key parameters to achieve closure. In a subsequent discussion, Dhir [60] pointed out that Gunnerson and Croenenberg's model predicts MHF values for subcooled water boiling on a sphere much higher than those measured experimentally, and the predictive accuracy worsens with increased subcooling. This points to weaknesses of the model in tackling, not only spherical surfaces, but flat surfaces as well, since predictions for the latter are based on those for spherical surfaces.

Recently, several Lattice-Boltzmann simulations were conducted by Cheng and co-workers [61–63] to generate a complete pool boiling curve for horizontal flat surfaces. Their results showed both MHF and T_{min} are influenced by surface wettability and thermal conductivities of the heating surface and the vapor.

To conclude, little theoretical modeling has been conducted to date that is robust enough in terms of capturing true interfacial behavior and accounting for all dominant parameters. One notable deficiency from most modeling efforts is the effect of surface condition, a topic worthy of significant attention in any future MHF study.

1.5. Objectives of present study

As is widely acknowledged, the MHF point is strongly influenced by both surface geometry and orientation, given the impact of these two parameters on vapor release and interfacial instabilities. Also, as discussed earlier, MHF is influenced by the liquid subcooling, however, in many applications, subcooling is avoided because of its tendency to increase residual stress, resulting in greater stress corrosion, hydrogen cracking and reduced fatigue strength [84].

The present pool boiling MHF-point analysis is dedicated to the most fundamental case of a horizontal flat surface with zero liquid subcooling. It is intended to serve as a baseline for future models addressing other complicating factors, including surface geometry and orientation, and liquid subcooling.

One key consideration in the present study is whether to focus the analysis on wall heat flux or wall temperature corresponding to the MHF point. By carefully reviewing available databases, the present authors uncovered appreciable scatter of MHF-point heat flux data from various sources under the same operating conditions, Fig. 2(a), compared to far less scatter for wall temperature data, Fig. 2(b). This observation is consistent with a conclusion drawn by Nishio et al. [85] regarding superiority of the temperature-controlled hypothesis to the heat-flux-controlled hypothesis in defining the MHF point. In other words, wall temperature is the better and more accurate determining factor. Therefore, the present study will focus on predicting the MHF-point wall temperature rather than the heat flux.

Table 2
Summary of theoretical models for pool boiling MHF point on horizontal flat surfaces.

Author(s)	Model rationale	Relevant formulae/Mechanisms
Thermodynamic models		
Spiegler *et al.* [64] (1963)	Equation of state	$T_{MS} = \frac{27}{32} T_c$
Lienhard [65] (1976)	van der Waals equation	$T_{MS} = T_c[0.905 + 0.095(T_{sat}/T_c)^8]$
Gunnerson & Cronenberg [66] (1978)	Transient contact	$T_{sat} < T_{min} \leq \frac{T_{MS}(\sqrt{k_w/\rho_w c_{pw}} + \sqrt{k_f/\rho_f c_{pf}}) - T_{MS}\sqrt{k_f/\rho_f c_{pf}}}{\sqrt{k_w/\rho_w c_{pw}}}$
Segev & Bankoff [67] (1980)	Langmuir monolayer adsorption	$\Lambda = \frac{\exp(Q_a/R_g T)}{\frac{(2\pi M R_g T)^{1/2}\Gamma_0}{P A_p \tau_0} + \exp(Q_a/R_g T)}$, where $\Gamma_0 = 10^{19}$ molecules/m^2 and $\tau_0 = 10^{-13}$ s, and T_{min} corresponds to $\Lambda = 0.9$.
Poniewski [68] (1987)	Nonequilibrium energy dissipation	T_{min} corresponds to equal equality of local potentials for liquid and vapor phases.
Olek *et al.* [69] (1988)	Zero contact angle hypothesis	$\cos\theta = 1 - C(T_{co} - T)^{b/(a-b)}/\sigma V_f$, where C is a constant, a and b are temperature-independent coefficients from a molecular force balance expression by Adamson [70].
Schroeder-Richter & Bartsch [71] (1990)	Thermo-mechanical effect	$h_g(T_g) - h_f(T_{min}) = 0.5[v_g(T_g) - v_f(T_{min})][P_{sat}(T_{min}) - P_{sat}(T_g)]$
Avedisian [72] (1985)	Homogeneous nucleation	$J = 1.44 \times 10^{40}(\frac{\rho_f^2\sigma}{M^3})^{1/2}\exp\{\frac{-1.213\times10^{24}\sigma^3}{T_f[\xi P_{sat}(T_f) - P_f]^2}\}$, where $\xi = \exp[\frac{P_f - P_{sat}(T_f)}{\rho_f T_f R_g}]$ and T_{MS} corresponds to $J = 10^{12}$ m^{-3}s^{-1}.
Carey [73] (1992)	Heterogenous nucleation	$J = 1.71 \times 10^{31}\frac{1+\cos\alpha}{2F}(\frac{M}{\rho_f})^{1/3}(\frac{\rho_f^2\sigma F}{M^3})^{1/2}\exp\{\frac{-1.213\times10^{24}F\sigma^3}{T_f[\xi P_{sat}(T_f) - P_f]^2}\}$, where $F = \frac{2+3\cos\alpha-\cos^2\alpha}{4}$, and T_{MS} corresponds to $J = 10^{10}$ m^{-2}s^{-1}.
Gerweck & Yadigaroglu [74] (1992)	Equation of state	T_{MS} is the minimum value of the local spinodal temperature.
Bernardin & Mudawar [75] (2002)	Bubble dynamics combined with surface characterization	$\Omega = 0.05\pi r_{max}^2(t)\frac{a_1}{a_2}\{\exp[-a_2 r_{min}(t)] - \exp[-a_2 r_{max}(t)]\}$, and T_{min} corresponds to $\Delta\Omega/\Delta t = 0.05$.
Aursand *et al.* [76] (2018)	Thermocapillary instability	$T_{min} = \frac{1}{3}T_{sat} + \frac{2}{3}T_{sat}[1 + \frac{9\sigma}{4+\mu_f/\mu_g}\frac{\sqrt{2\pi R_g T_{sat}}}{k_g f(\varepsilon)}]^{1/2}$, where $f(\varepsilon)$ is a function of the evaporation coefficient ε.
Hydrodynamic models		
Zuber [55] (1959)	Rayleigh-Taylor instability	$MHF = \frac{\pi^2}{60}(\frac{4}{3})^{1/4}\rho_g h_{fg}[\sigma g\frac{\rho_f - \rho_g}{(\rho_f + \rho_g)^2}]^{1/4}$
Sanders & Colver**	Corresponding state theory	$MHF = 11.2(10^6)[\lvert P\rvert]^{0.468}(P_R - P_{tp}/P_c)(1 - P_R)^{0.827}[P_c(R_g g_c T_c/M)^{1/2}]$
Kutateladze** [77] (1959)	Equations of motion	$MHF = Ch_{fg}(g\rho_g\frac{\rho_f + \rho_g}{\rho_f})^{1/2}[\frac{\sigma g_c(\rho_f - \rho_g)}{g}]^{1/4}$, where C is a constant.
Berenson [56] (1961)	Taylor-Helmholtz instability	$MHF = 0.09\rho_g h_{fg}[\sigma g\frac{\rho_f - \rho_g}{(\rho_f + \rho_g)^2}]^{1/4}$
Morozov** [78] (1963)	Dimensional analysis	$T_{min,B} = T_{sat} + 0.127\frac{\rho_g h_{fg}}{k_g}(g\frac{\rho_f - \rho_g}{\rho_f + \rho_g})^{2/3}[\frac{\sigma}{g(\rho_f - \rho_g)}]^{1/2}[\frac{\mu_g}{g(\rho_f - \rho_g)}]^{1/3}$
Ruckenstein [79] (1967)	Taylor instability & bubble growth	$MHF = 0.0267\rho_g h_{fg}(\sigma g\frac{\rho_f - \rho_g}{\rho_g^2})^{1/4}$
Henry [57] (1974)	Modified Berenson's model	$MHF = C\rho_g h_{fg}[\sigma g\frac{\rho_f - \rho_g}{(\rho_f + \rho_g)^2}]^{1/4}$, where C is a constant whose magnitude depends on initial and final radii of the bubble prominence.
Lienhard & Dhir [80] (1980)	Rayleigh-Taylor instability	$T_{min} = T_{min,B} + 0.42(T_{min,B} - T_f)(\frac{k_f\rho_f c_{pf}}{k_w\rho_w c_{pw}})^{3/10}[\frac{h_{fg}}{c_{pw}(T_{min,B} - T_{sat})}]^{3/5}$
Gunnerson & Cronenberg [58, 59] (1980)	Transient contact	$MHF = 0.091^{0.078}_{0.104}\rho_g h_{fg}[\sigma g\frac{\rho_f - \rho_g}{(\rho_f + \rho_g)^2}]^{1/4}$
Sher *et al.* [81] (2012)	Rayleigh-Taylor instability	$MHF = \rho_g(h_{fg} + c_{pl}\Delta T_{sub} + c_{pg}\Delta T_{sup})\frac{\pi d^3}{6\lambda^2}f_{min} + \frac{2.3k_f\Delta T_{sub}f_{min}^{1/2}}{(\pi\alpha_f)^{1/2}} + \frac{2k_f(T_i - T_f)t_{tc}^{1/2}A_{tc}f_{min}}{(\pi\alpha_f)^{1/2}\lambda^2}$
Kim *et al.* [82] (2015)	Rayleigh-Taylor instability	$MHF = \frac{\pi C}{6}(\frac{2}{3})^{1/2}\rho_g h_{fg}[\sigma g\frac{\rho_f - \rho_g}{(\rho_f + \rho_g)^2}]^{1/4}$, where C is an empirical constant.
		$MHF = [\frac{2^{1/2}\pi C}{24}k_g^3\Delta T_{min}^3\frac{\rho_g(\rho_f - \rho_g)^{3/2}g^{3/2}h_{fg}}{\sigma^{1/2}\mu_g}]^{1/4}$, where C is a function of bubble diameter at breakoff, release frequency, and bubble spacing. For water, $\Delta T_{min} = \min[150, T_{MS} - T_{sat}]$.

** As referenced by Clements & Colver [83] (1970)

2. Heat transfer coefficient for pool film boiling

Heat transfer during pool film boiling on a horizontal surface is highly dependent on the mechanism of vapor release from the heating wall. This process has been studied extensively in the past few decades, with many Nusselt number models and correlations recommended, as shown in Table 3, to determine the heat transfer coefficient. It should be noted that different length scales have been used to define the Nusselt number. To ensure uniformity when comparing dimensionless groups, the two-dimensional critical Taylor wavelength is used, *i.e.*, $Nu = h\lambda_c/k_g$. Therefore, some of the relations in this table may be somewhat different from their original form.

Two of the most widely adopted Nusselt number expressions are the mechanistic model proposed by Berenson [56] and empirical correlations by Klimenko [86]. Both have shown satisfactory agreement against numerical predictions [87] and experimental results [88]. Berenson's formulation was constructed around the Taylor-Helmholtz hydrodynamic instability for laminar vapor flow along the surface with a regularly distributed bubble release. Using the assumption that both the distance between adjacent vapor bubbles and the departure diameter are proportional to the criti-

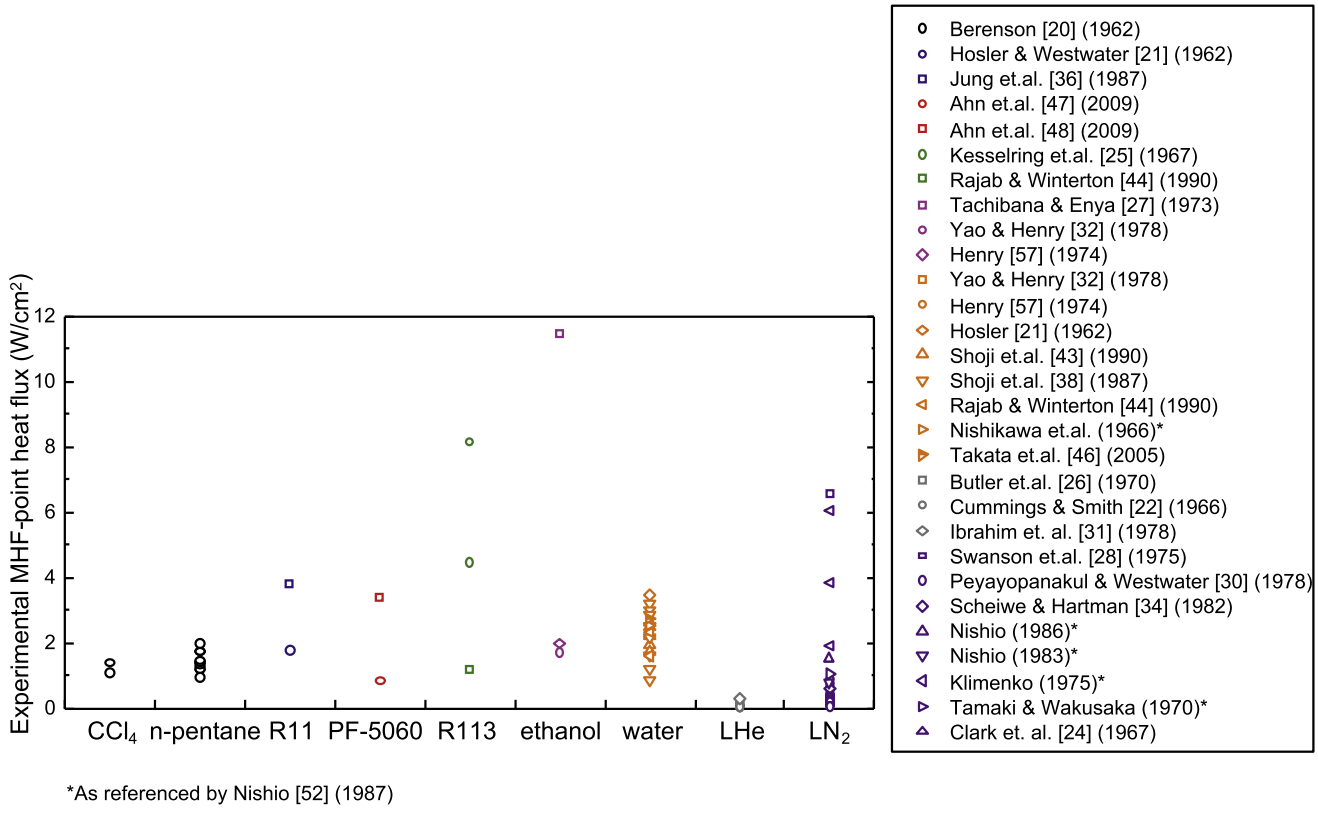

(a)

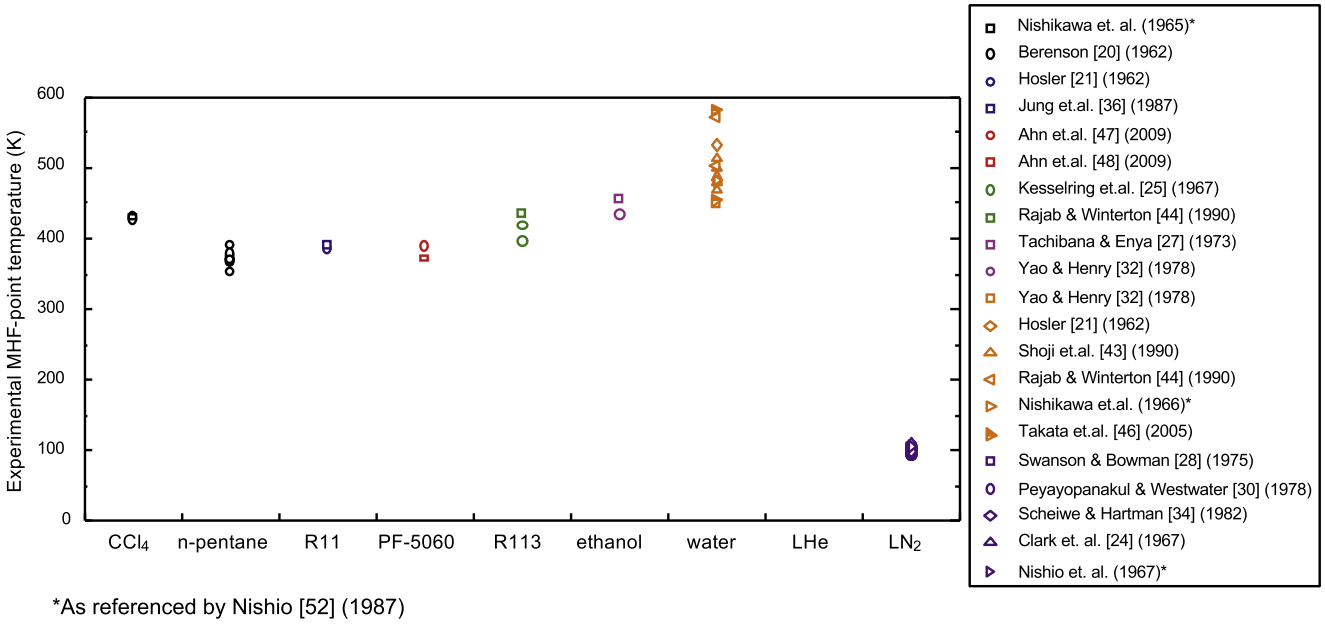

(b)

Fig. 2. Deviations of MHF-point's (a) wall heat flux data and (b) wall temperature data for saturated pool boiling on flat horizontal surfaces at atmospheric pressure.

cal Taylor wavelength, he constructed a semi-empirical model for area-averaged film boiling heat transfer coefficient, which required fitting the value of an unknown multiplier in his final relation using his own experimental data.

Using the same basic physical mechanism as Berenson's, the generalized correlations by Klimenko were derived for both laminar and turbulent vapor film flows using Reynolds' heat transfer analogy. Klimenko's relations have been validated against experimental data from fifteen different sources for a variety of both normal and cryogenic fluids and pressures ranging from atmospheric to near-critical [86, 89]. Extended applicability to different fluids renders Klimenko's formulation a more superior choice for predict-

Table 3
Heat transfer coefficient relations for saturated pool film boiling on a horizontal upward-facing surface.

Author(s)	Relevant formulae	Notes
Chang [97] (1959)	$Nu = 0.294(\alpha Ra_g)^{1/3}$	$Ra_g = \frac{g\lambda_c^3}{\nu_g^2}\mathrm{Pr}_g(\rho_f/\rho_g - 1)$, $\alpha = \frac{h'_{fg}}{c_{pg}\Delta T_{sup}}$, $\mathrm{Pr}_g = \mu_g c_{pg}/k_g$
Berenson [56] (1961)	$Nu = 0.673(\alpha Ra_g)^{1/4}$	$h'_{fg} = h_{fg}(1 + 0.50c_{pg}\Delta T_{sup}/h_{fg})$
Brentari & Smith*** (1965)	$Nu = 0.811(\alpha Ra_g)^{1/4}$	$h'_{fg} = h_{fg}(1 + 0.50c_{pg}\Delta T_{sup}/h_{fg})$
Padilla [23] (1966)	$Nu = 0.909(\alpha Ra_g)^{1/4}$	$h'_{fg} = h_{fg}(1 + 0.50c_{pg}\Delta T_{sup}/h_{fg})$
Hamill & Baumeister [98] (1966)	$Nu = 0.649(\alpha Ra_g)^{1/4}$	$h'_{fg} = h_{fg}(1 + 0.95c_{pg}\Delta T_{sup}/h_{fg})$
Frederking *et al.* [99] (1966)	$Nu = 0.20(\alpha Ra_g)^{1/3}$	$h'_{fg} = h_{fg}(1 + 0.50c_{pg}\Delta T_{sup}/h_{fg})$
Clark *et al.* [24] (1967)	$Nu = 0.012(\alpha Ra_g)^{1/2}$	$h'_{fg} = h_{fg}(1 + 0.50c_{pg}\Delta T_{sup}/h_{fg})$
Lao *et al.* [100] (1970)	$Nu = 185\mathrm{Pr}_g\alpha^{-0.09}$	$h'_{fg} = h_{fg}$
Klimenko [86] (1981)	$Nu = \begin{cases} 0.19[Ga_g(\rho_f/\rho_g - 1)]^{1/3}\mathrm{Pr}_g^{1/3} f_1 & 7\times10^4 < Ga_g(\rho_f/\rho_g - 1) < 10^8 \\ 0.0086[Ga_g(\rho_f/\rho_g - 1)]^{1/2}\mathrm{Pr}_g^{1/3} f_2 & 10^8 < Ga_g(\rho_f/\rho_g - 1) < 3\times10^8 \end{cases}$	$f_1 = \begin{cases} 1 & \alpha \le 1.4 \\ 0.89\alpha^{1/3} & \alpha > 1.4 \end{cases}$, $f_2 = \begin{cases} 1 & \alpha \le 2.0 \\ 0.71\alpha^{1/2} & \alpha > 2.0 \end{cases}$, $h'_{fg} = h_{fg}$
		$Ga_g = g\lambda_c^3/\nu_g^2$, for $P/P_c = 0.0045 - 0.98$, $\alpha = 0.031 - 7.3$and $\mathrm{Pr}_g = 0.69 - 3.45$
Tanaka [101] (1988)	$Nu = 1.822(\frac{\rho_f}{\rho_f - \rho_g})^{2/5}(\alpha Ra_g)^{1/5}$	$h'_{fg} = h_{fg}$
Dhir [102] (2001)	$Nu = 0.42[Gr_g\mathrm{Pr}_g(\alpha + 0.5 + 1.3\alpha^{-1/4})]^{1/4}$	$Gr_g = \frac{g\beta_T\Delta T_{sup}}{\nu_g^2}(\frac{\lambda_c}{2\pi})^3$,
		$\mathrm{Pr}_g = 0.72 - 420$,$\alpha = 0.007 - 11.1$,$Gr_g = 210 - 2.2\times10^6$, $h'_{fg} = h_{fg}$
Zhang & Murakami [103] (2005)	$Nu = (0.58 + 0.07\frac{\lambda_c}{D'})(\alpha Ra_g)^{1/4}$	$h'_{fg} = h_{fg}(1 + 0.34c_{pg}\Delta T_{sup}/h_{fg})^2$, D' is the ratio of surface area to the perimeter.

*** As referenced by Sauer & Ragsdell [104] (1971)

ing the heat transfer coefficient for film boiling than the Berenson model. Additionally, numerical simulations have shown the Klimenko method provides better predictions than Berenson's [90–95], especially for cryogens [96].

It is widely acknowledged that the characteristic length of the heating surface, such as diameter or width, has an appreciable influence on the heat transfer characteristics for very small surfaces. Therefore, a surface size threshold must be exceeded for the *Nu* correlations for an infinite horizontal flat surface to be valid. For a heating surface with 'minimum size' D (diameter for a circular surface or shortest side length for a rectangular surface), Klimenko [86] proposed using a threshold five times the critical Taylor wavelength to demarcate Nusselt number expressions for large (infinite) versus small surfaces,

$$\frac{Nu'}{Nu} = \begin{cases} 1 & D > 5\lambda_c \\ 2.90(\lambda_c/D)^{0.67} & D \le 5\lambda_c \end{cases}, \quad (1)$$

Accounting for heater size effects represents a key advantage of the Klimenko method compared to Berenson's. This is why the model presented in this paper will rely on film boiling heat transfer coefficient predictions based on the former.

However, it must be noted that neither Klimenko's or Berenson's methods account for the spatial and temporal variations of wall temperature or vapor film thickness. Therefore, neither method can predict local, transient heat transfer characteristics during film boiling.

3. Pool boiling MHF-point model development

For saturated pool film boiling (*i.e.,* at wall temperatures exceeding the MHF-point temperature) on a horizontal surface, the vapor-liquid interface exhibits a well-defined instability pattern, combined with a vapor release mechanism. Analysis of the vapor film dynamics in film boiling is an intuitive approach to explaining the MHF point as a limiting condition for film boiling. In the present paper, a mechanistic model is developed to describe this limit.

3.1. Model assumptions

For horizontal pool film boiling, the liquid phase overlays the vapor phase in a gravitational field. In view of the complexity of the MHF-point mechanism, the model is based on several simplifying assumptions:

(1) Both the liquid and vapor phases are incompressible.
(2) The surface is flat, horizontal, and infinite.
(3) Liquid temperature is equal to saturation temperature corresponding to the system's operating pressure.
(4) The heating surface possesses a sufficiently high thermal mass that its temperature remains constant for a given heat flux.
(5) Phase change occurs only along the liquid-vapor interface.
(6) Radiation effects are negligible.
(7) Thickness of the vapor film is larger than any surface roughness features.

Assumption (6) is justified by the fact that most surfaces employed in MHF experiments are polished and therefore possess very low emissivity. Additionally, calculations by the present authors show that the radiation heat flux is less than 3% of the measured MHF. And, regarding assumption (7), it should be noted that, although vapor film thickness decreases as wall temperature is decreased from film boiling to the MHF point, the roughness features for flat surfaces for which the present model is intended are typically much smaller than the vapor layer thickness. However, this may not be true for enhanced surfaces having surface elements traversing the entire vapor layer. The MHF mechanism for such enhanced surfaces is beyond the scope of the present baseline model.

3.2. Unit cell of vapor film

Depicted in Fig. 3 is a schematic of the liquid-vapor interface for stable film boiling on an infinite horizontal surface. When the wall temperature is higher than that corresponding to the MHF-point, a thin continuous vapor film forms between the bulk saturated liquid and the heating surface, which prevents direct liquid contact with the surface. Phase change occurs at the liquid-vapor interface due to heat conduction from the heating surface across the vapor film. Gravity induces instability along the interface, creating a wavy vapor film with valleys and peaks, and causing the vapor accumulated beneath the liquid to flow from the valleys to the peaks. Appreciable vapor formation within the film boiling regime triggers vapor release from the vapor peaks.

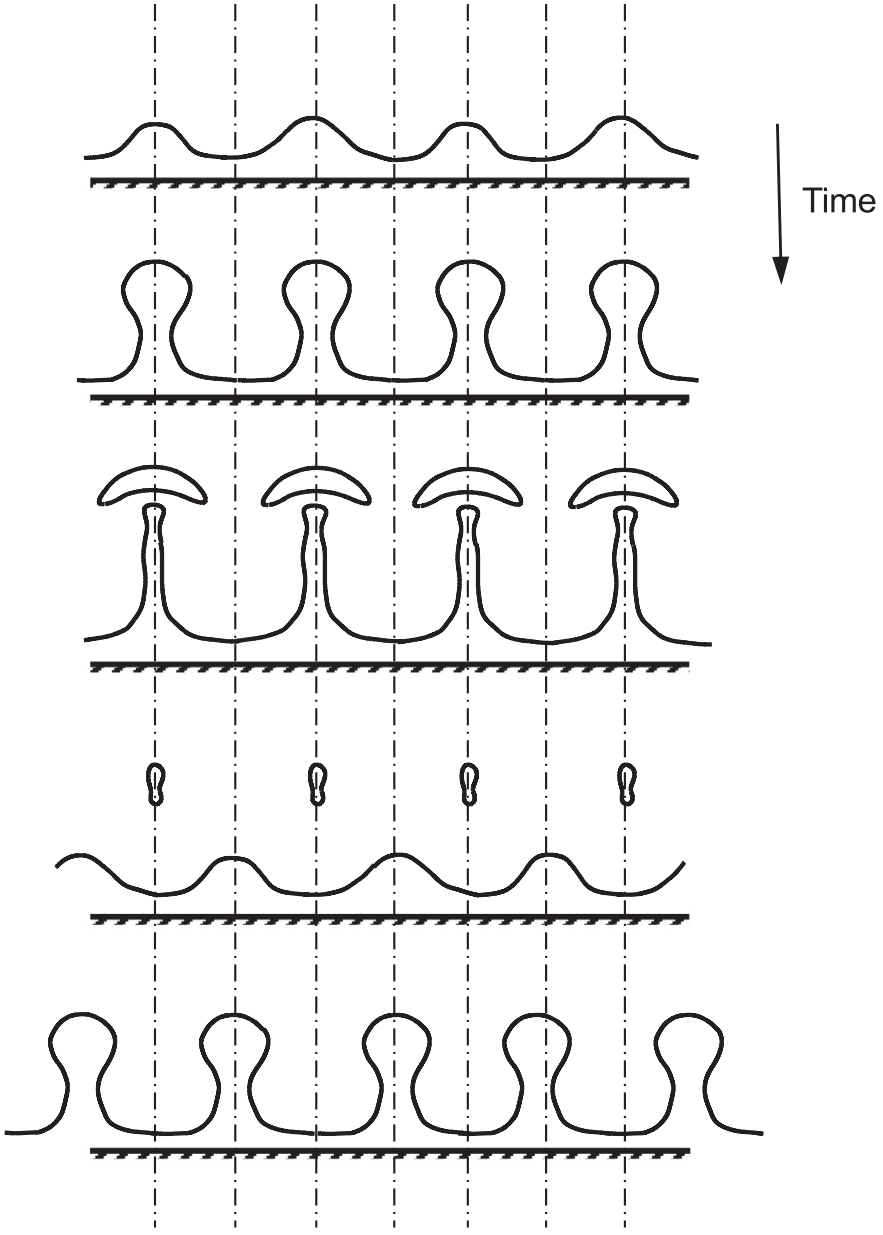

Fig. 3. Schematic of the liquid-vapor interface during stable pool film boiling on a flat infinite horizontal heating surface.

Overall, the vapor generated in the vapor film valley is absorbed entirely by two adjacent peaks, which points to the formation of a series of repeated unit cells. This implied vapor formation along the entire surface may be modeled by focusing on a single representative unit cell.

Previous experiments [21] verified that film boiling from a horizontal surface follows the Taylor instability, which is induced by gravity along the interface between two low velocity fluids in which high density liquid resides above low density vapor. Absence of inertia effects on the interfacial instability in the same experiments points to very low vapor velocities, especially at the MHF point.

Within a single unit cell, the distance between adjacent vapor peaks is assumed to equal the critical Taylor wavelength,

$$\lambda_c = 2\pi \sqrt{\frac{\sigma}{g\left(\rho_f - \rho_g\right)}}, \tag{2}$$

which is dominated by a balance between buoyancy and surface tension. Disturbances with wavelengths greater than the critical value will amplify and eventually lead to unstable vapor rupture.

In the subsequent sections, a force balance will be applied to the unit cell in a direction normal to the heating surface, including effects of pressure difference, surface tension, and normal vapor momentum flux.

3.2.1. Pressure difference

According to classical instability theory [105], an idealized vapor-liquid interface is shown in Fig. 4 as a simple harmonic wave with interfacial displacement given by

$$\eta(z,t) = \eta_0 \exp\left[ik(z - ct)\right], \tag{3}$$

where η_0 is the wave amplitude, which is assumed to be equal to the mean vapor layer thickness δ, and k and c are, respectively, the wave number ($k = 2\pi/\lambda$) and wave speed. The wave speed has both real and imaginary components (*i.e.*, $c = c_r + \mathbf{i}c_i$), with

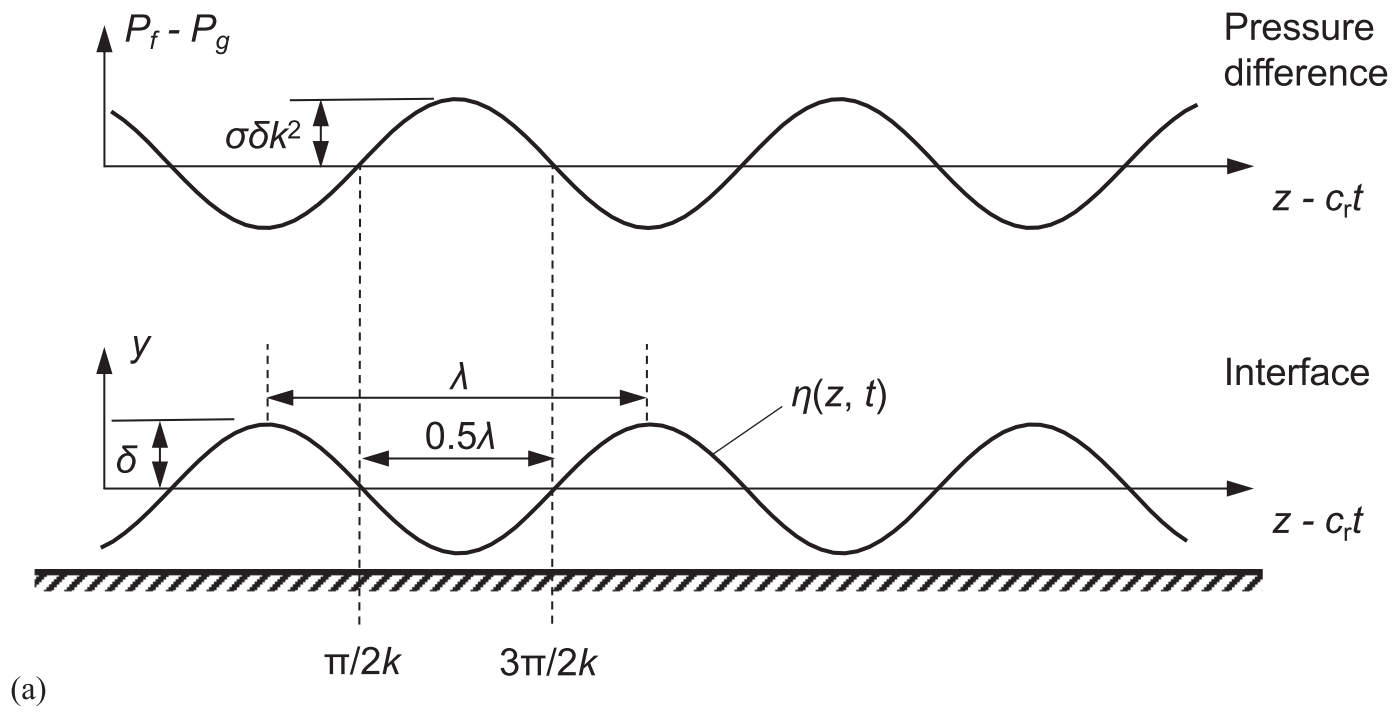

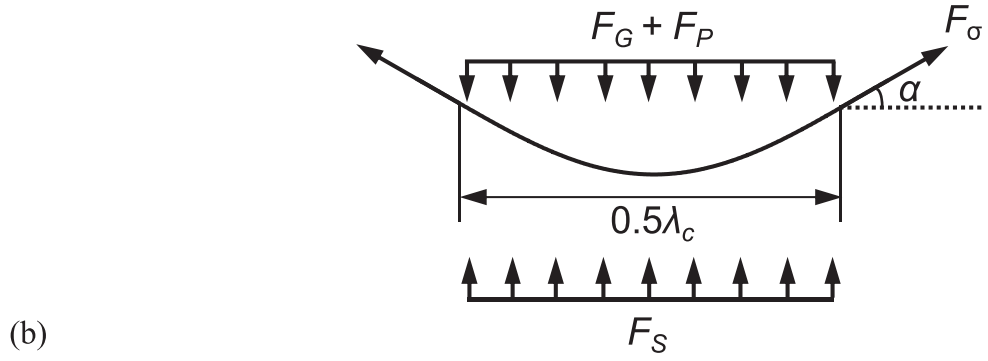

Fig. 4. (a) Plots of pressure difference across the interface and interfacial displacement. (b) Force balance for the half wavelength trough region of the unit cell.

the former representing the actual interface speed while the latter providing a criterion for interfacial stability.

Assuming the system is inviscid, irrotational and incompressible, instability analysis indicates pressure difference perpendicular to the interface can be expressed as

$$P_f - P_g = \sigma \left\{ \left[1 + \left(\frac{\partial \eta}{\partial z} \right)^2 \right]^{3/2} / \frac{\partial^2 \eta}{\partial z^2} \right\}^{-1} \approx \sigma \frac{\partial^2 \eta}{\partial z^2} = -\sigma k^2 \eta \,. \quad (4)$$

With only a real component of wave speed, c_r, the interface evolves periodically and is therefore stable. On the other hand, with a finite imaginary component, c_i, an interfacial disturbance would grow exponentially with time. At the onset of instability (corresponding to $c_i = 0$), the interfacial curvature can be expressed as a simple sinusoid,

$$\eta(z,t) = \delta \cos[k_c(z - c_r t)] \,. \quad (5)$$

Substituting Eq. (5) into Eq. (4) and integrating the pressure difference over the trough region with half wavelength yield the following expression for pressure force across the interface:

$$F_P = \int_{\pi/2k_c}^{3\pi/2k_c} -\sigma k_c^2 \delta W \cos[k_c(z - c_r t)] d(z - c_r t) = 2\sigma k_c \delta W, \quad (6)$$

where W is the width of the heating wall perpendicular to the page depicted in Fig. 3.

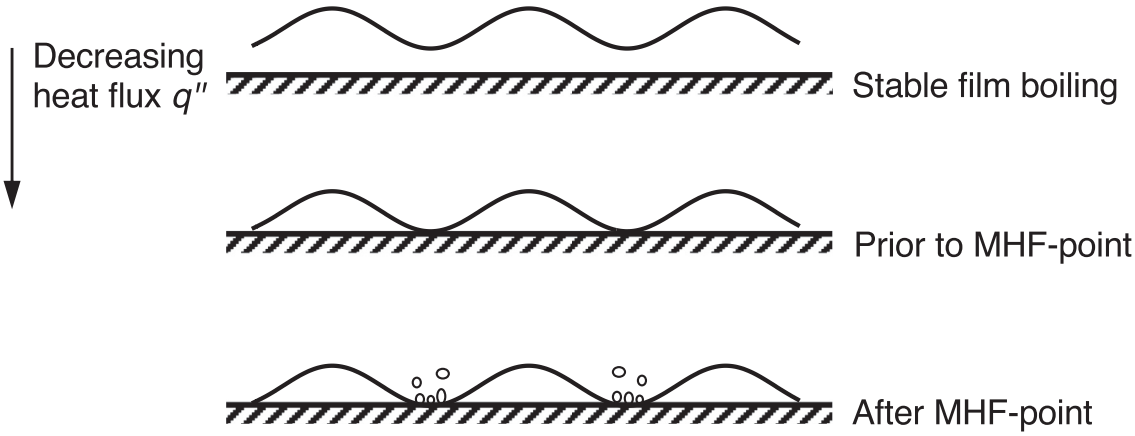

Fig. 5. Schematic representation of initiation of the MHF condition.

3.2.2. Surface tension force

Surface tension plays a vital role in terms of providing interfacial stability. As shown in Fig. 4, the net surface tension force acting on the half wavelength trough region of the unit cell in the direction normal to the heating surface is given by

$$F_\sigma = 2\sigma W \sin(\pi/4). \tag{7}$$

3.2.3. Gravitational force

For pool film boiling on a flat horizontal surface, the denser liquid is suspended above much lower density vapor, which is why buoyancy is both destabilizing to the interface and aids in promoting interfacial contact with the heating surface. The gravitational force is determined as follows,

$$F_G = \int_{\pi/2k_c}^{3\pi/2k_c} -\left(\rho_f - \rho_g\right) gW\delta \cos\left[k_c(z - c_r t)\right] d(z - c_r t) = \frac{2gW\delta}{k_c}\left(\rho_f - \rho_g\right). \tag{8}$$

3.2.4. Stagnation pressure force

In the present model development, it is assumed film boiling is terminated and the MHF condition initiated once liquid begins contacting the heating wall. This causes sudden vapor formation normal to the wall. An energy balance is applied to the half wavelength trough region, in which the wall heat flux q" converts the liquid to saturated vapor.

$$\rho_g h_{fg} U_{g,n} SW = 0.5\lambda_c q'' W, \tag{9}$$

where $S = 0.5\lambda_c$ for simplicity, and $U_{g,n}$ is vapor velocity normal to the interface.

At the heating surface, the vapor velocity goes to zero and therefore creates additional stagnation pressure, F_S, along the underside of the interface, which can be expressed as $0.5\rho_g U_{g,n}^2$ according to Bernoulli's equation. Summation of stagnant pressure along the vapor trough yields

$$F_S = \frac{1}{4}\rho_g \left(\frac{q''}{\rho_g h_{fg}}\right)^2 \lambda_c W, \tag{10}$$

3.3. Physical mechanism for MHF point

As shown in Fig. 5, in the stable film boiling regime, a continuous vapor film insulates the heating surface. With a decrease in wall heat flux towards the MHF point, liquid approaches the heating surface but without wetting. A further decrease in heat flux triggers the MHF condition as the downward forces pushing the interface towards the wall overcome the upward forces lifting the interface away from the wall. This causes the wavy liquid-vapor interface to contact and wet the heating surface; vigorous bubble nucleation and vapor production ensue, signaling onset of the transition boiling regime.

By focusing on the half wavelength trough region of the interface, it is obvious that the dominant interfacial stabilizing terms are those associated with surface tension and stagnation pressure on the underside of the interface, and the destabilizing terms are those of gravity and pressure difference across the curved interface. The interface will maintain separation from the heating wall (*i.e.,* film boiling) so long as the stabilizing forces exceed the destabilizing ones. The MHF condition is reached when the two sets of terms are in equilibrium,

$$\frac{1}{4}\rho_g \left(\frac{q''_{\min}}{\rho_g h_{fg}}\right)^2 \lambda_c W + 2\sigma W \sin\frac{\pi}{4} = 2\sigma k_c \delta W + \frac{2gW\delta}{k_c}\left(\rho_f - \rho_g\right). \tag{11}$$

Rearranging terms in Eq. (11) provides the final expression for MHF,

$$q''_{\min} = 2\rho_g h_{fg}\left[4\pi \frac{\sigma\delta}{\rho_g \lambda_c^2} + \frac{g\lambda_c \delta\left(\rho_f - \rho_g\right) - \sqrt{2}\pi\sigma}{\pi\rho_g \lambda_c}\right]^{1/2}. \tag{12}$$

3.4. Determination of MHF-point wall temperature

Since the vapor film thickness δ in Eq. (12) exhibits appreciable temporal and spatial variation along the heating surface, it is quite difficult to assign a specific value for use in the MHF model. An alternative method is adopted to resolve this issue. It is obvious that the heat flux corresponding to the MHF point is much smaller than that for fully developed film boiling. Assuming the value of heat flux in Eq. (12) is comparatively very small, the vapor film thickness approaches a clearly defined limit,

$$\delta|_{q''\to 0} \to \frac{\sqrt{2}\sigma}{\frac{4\pi\sigma}{\lambda_c} + \frac{g\lambda_c\left(\rho_f - \rho_g\right)}{\pi}}. \tag{13}$$

It is assumed that, at the MHF point, there is an increase in the vapor film thickness that is proportional to the above limit,

$$\Delta\delta = \chi\, \delta|_{q''\to 0}. \tag{14}$$

That is, the vapor film thickness at the MHF point is given by

$$\delta|_{q''_{\min}} = (1 + \chi)\, \delta|_{q''\to 0}. \tag{15}$$

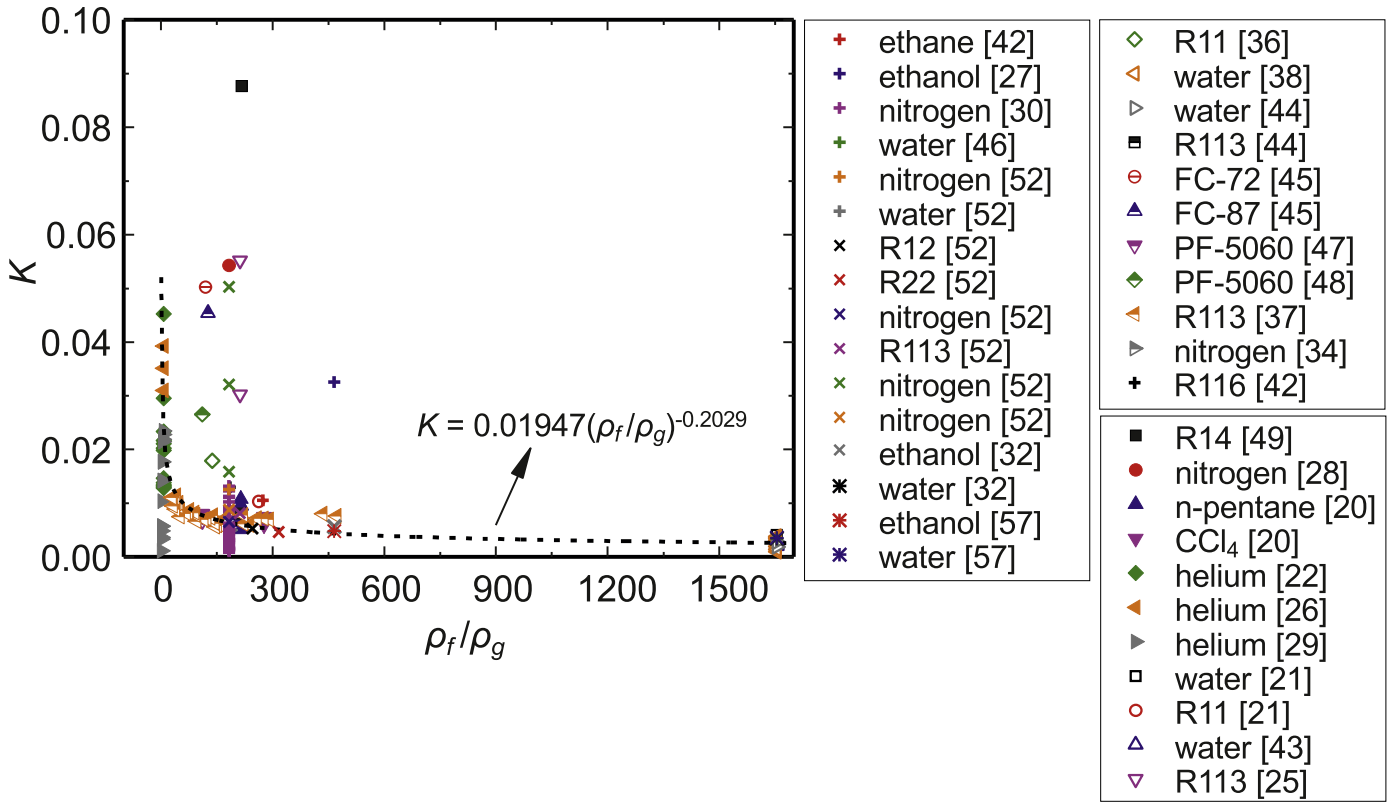

Fig. 6. Correlation of K values to density ratio for different fluids.

Substituting Eq. (13) into Eq. (15) yields the following expression for the minimum heat flux:

$$q''_{\min} = 2\rho_g h_{fg}\left(\chi\frac{\sqrt{2}\sigma}{\rho_g\lambda_c}\right)^{1/2}. \tag{16}$$

Introducing the expression in Eq. (2) for the critical Taylor wavelength, Eq. (16) becomes

$$q''_{\min} = \frac{2\times 2^{1/4}}{(2\pi)^{1/2}}\chi^{1/2}\rho_g h_{fg}\left[\frac{\sigma g(\rho_f-\rho_g)}{\rho_g^2}\right]^{1/4}. \tag{17}$$

To account for the pressure effect on the MHF condition, it is assumed that χ is related to the density ratio of liquid and vapor, *i.e.*,

$$\chi \sim \left(\frac{\rho_f}{\rho_g}\right)^{m_2}. \tag{18}$$

Then, the minimum heat flux in Eq. (17) can be expressed as

$$q''_{\min} = m_1\left(\frac{\rho_f}{\rho_g}\right)^{m_2/2}\rho_g h_{fg}\left[\frac{\sigma g(\rho_f-\rho_g)}{\rho_g^2}\right]^{1/4}, \tag{19}$$

where m_1 and m_2 are constants.

Eq. (19) can finally be rearranged to yield the following non-dimensional form for the minimum heat flux,

$$K = \frac{q''_{\min}}{\rho_g h_{fg}\left[\frac{\sigma g(\rho_f-\rho_g)}{\rho_g^2}\right]^{1/4}} = m_1\left(\frac{\rho_f}{\rho_g}\right)^{m_2/2}. \tag{20}$$

As shown in Fig. 6, using available experimental data for a large number of fluids, the value of K in Eq. (20) can be correlated directly to density ratio, resulting in the following final expression for minimum heat flux:

$$q''_{\min} = 0.01947\left(\frac{\rho_f}{\rho_g}\right)^{-0.2029}\rho_g h_{fg}\left[\frac{\sigma g(\rho_f-\rho_g)}{\rho_g^2}\right]^{1/4}. \tag{21}$$

The above model derivation yields an expression for minimum heat flux rather than wall temperature. However, as shown in Fig. 2, the measured minimum heat flux values available from different sources (and even the same source) under identical conditions exhibit very large scatter. On the other hand, wall temperature corresponding to the MHF point shows far better consistency between different sources. Therefore, by setting

$$q''_{\min} = h(T_{\min}-T_{sat}) = \frac{k_g}{\lambda_c}Nu_g(T_{\min}-T_{sat}) \tag{22}$$

and using the Nusselt number relations by Klimenko [86] (see Table 3), a final expression for MHF-point wall temperature is achieved,

$$T_{\min} = T_{sat} + 0.1223\left(\frac{\rho_f}{\rho_g}\right)^{-0.2029}\frac{\rho_g h_{fg}}{Nu_g k_g}\left[\frac{\sigma^3}{g\rho_g^2(\rho_f-\rho_g)}\right]^{1/4}. \tag{23}$$

Lastly, it is important to note that all the above relations are applied to a continuous vapor film, *i.e.*, approaching the MHF-point condition from the film boiling regime rather than from transition boiling.

4. Results and discussion

4.1. Comparison of model predictions with experimental data

Two primary goals of this section are to (1) assess the predictive accuracy of the present model against experimental data for minimum wall temperature, and (2) compare the predictive capability of the model against those of prior models. Both goals

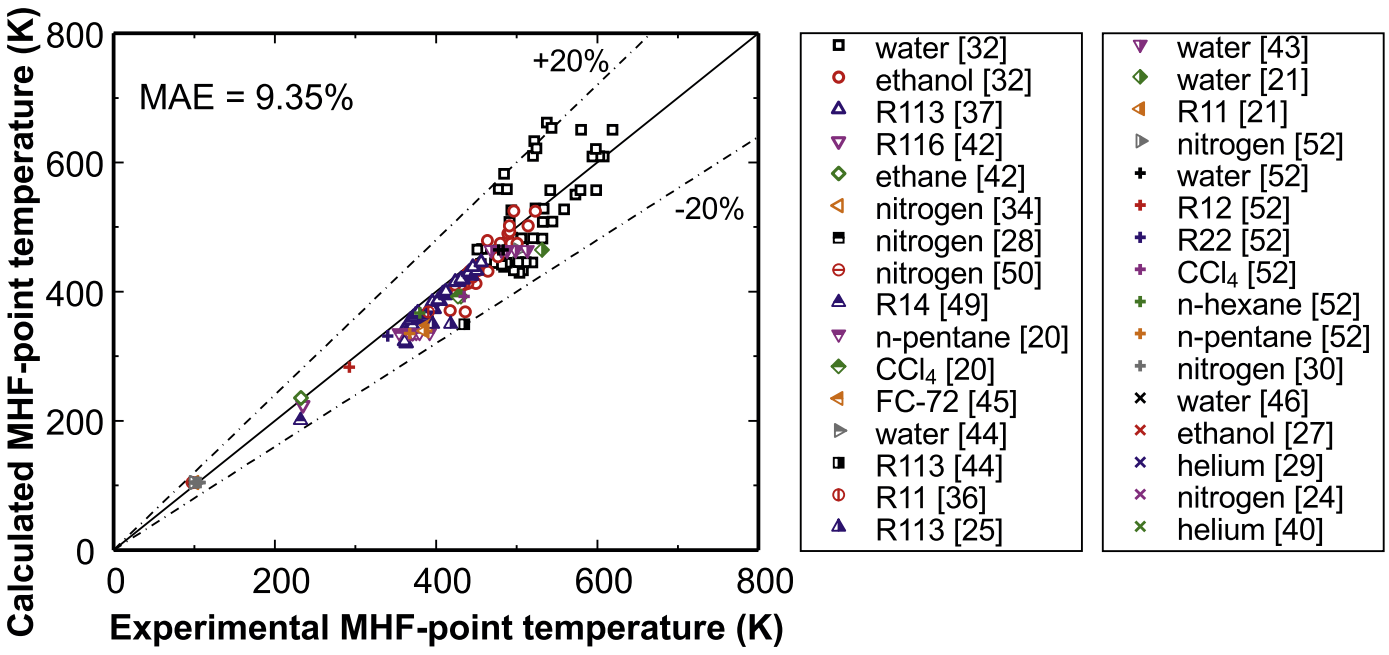

Fig. 7. Comparison of MHF-point wall temperature predicted by the present model with experimental data.

are achieved by comparing predictions to a consolidated minimum wall temperature database. When conducting these comparisons, thermos-physical properties for different working fluids are obtained using NIST's REFPROP 8.0 software [106], excepting those for FC-72, FC-87 and PF-5060, which are obtained from 3M Company.

For the MHF-point conditions, the previous study found very little differences between vapor properties estimated at saturation temperature and those evaluated at the average of saturation and wall temperatures [82]. Therefore, for simplicity, all vapor and liquid properties are evaluated at saturation temperature corresponding to measured system pressure.

In the present study, a total of 233 data points of saturated pool boiling MHF-point wall temperature for a horizontal upward-facing flat surface are amassed from 27 sources. The data are obtained either directly from the original sources or extracted by digitalizing data plots using commercial software. It should be mentioned that the data used here are carefully selected based on availability of all parameters needed to execute the calculations. Therefore, some data provided by sources in Table 1 are not used in the comparison. Examples of excluded data include those of superfluid helium II [33], which display peculiar trends (*e.g.*, strong depth effects and appreciable noise in film boiling), and liquid metal potassium [23], for which vapor density values are lacking.

The overall accuracy of predictions is assessed using mean absolute error (MAE), which is defined as

$$\mathrm{MAE} = \frac{1}{n}\sum \frac{\left|T_{\min,\exp} - T_{\min,\mathrm{pred}}\right|}{T_{\min,\mathrm{pred}}} \times 100\%, \tag{23}$$

where n is the total number of data points.

Fig. 7 compares predicted and measured MHF-point wall temperatures for different liquids and pressures. It shows fairly good predictive accuracy, evidenced by a MAE of 9.35%. Considering data for only normal fluids (*i.e.,* neglecting all cryogen data), the MAE decreases to 6.36%. This provides strong validation support for the model's mechanistic approach over the entire range of liquid types and pressures. Deviations between the predictions and data may be attributed to a couple of factors: (1) influence of solid wall thermal properties, which are not accounted for in the model, and (2) influence of 3D interfacial wave effects, which are simplified in the present model using 2D wave analysis.

However, although not obvious from Fig. 7, the calculated results show poorer agreement (MAE = 43.10%) with the liquid helium data (LHe). Such disagreement is somewhat expected because both saturation temperature and measured wall temperature for liquid helium are extremely low, so is the measured difference between wall and saturation temperatures. For example, for a difference between measured and calculated MHF-point wall temperatures of only 1 K, the MAE for LHe is more than 15%, compared to ~0.2% for water. In other words, experimental error in liquid helium experiments is often unusually high. Furthermore, wall temperature for the same fluid is higher than the critical point temperature for most cases, and vapor very close to the surface may exhibit unusual property variations. However, because of much higher saturation temperature for liquid nitrogen (LN_2), predictions for this cryogen (MAE = 4.98%) are quite satisfactory.

4.2. Assessment of previous models

In this section, predictive accuracies of 4 previous models intended for the horizontal, upward-facing flat surfaces are also assessed. Thermophysical properties of the metallic solid wall used in the calculations are provided in Table 4. Fig. 8 compares the MAEs of the 4 models using the same database as in Section 4.1. However, fewer data points are used in specific comparisons. For example, some data sources do not include solid wall alloy, thermophysical properties for which are needed when using Henry's model [57]. Additionally, some of the data [107-110] are extracted from another source [52] without specifying solid wall material.

Table 5 lists detailed MAEs of the 4 models alongside those of the present model. Overall, best predictions are achieved with the thermodynamic model by Spiegler *et al.* [64] (MAE = 8.94%), followed in order by the present model (MAE = 9.35%), Lienhard's thermodynamic model [65] (MAE = 13.24%), Berenson's hydrodynamic model [56] (MAE = 77.20%), and Henry's [57] hydrodynamic model (MAE = 86.67%). Interestingly, despite being widely used and recommended, Berenson's and Henry's hydrodynamic mod-

Table 4
Representative thermophysical properties of solid metal walls [111].

Wall material	Density ($kg \cdot m^{-3}$)	Thermal conductivity ($W \cdot m^{-1} \cdot K^{-1}$); specific heat ($J \cdot kg^{-1} \cdot K^{-1}$)				
	300 K	100 K	200 K	300 K	400 K	600 K
Aluminum	2702	302; 482	237; 798	237; 903	240; 949	231; 1033
Copper	8933	482; 252	413; 356	401; 385	393; 397	379; 417
Gold	19300	327; 109	323; 124	317; 129	311; 131	298; 135
Inconel	8510	10.3; 372	13.5; 473	11.7; 439	20.5; 546	24.0; 626
Nickel	8900	164; 232	107; 383	90.7; 444	80.2; 485	65.6; 592
Stainless steel	7900	9.2; 272	12.6; 402	14.9; 477	16.6; 515	19.8; 557

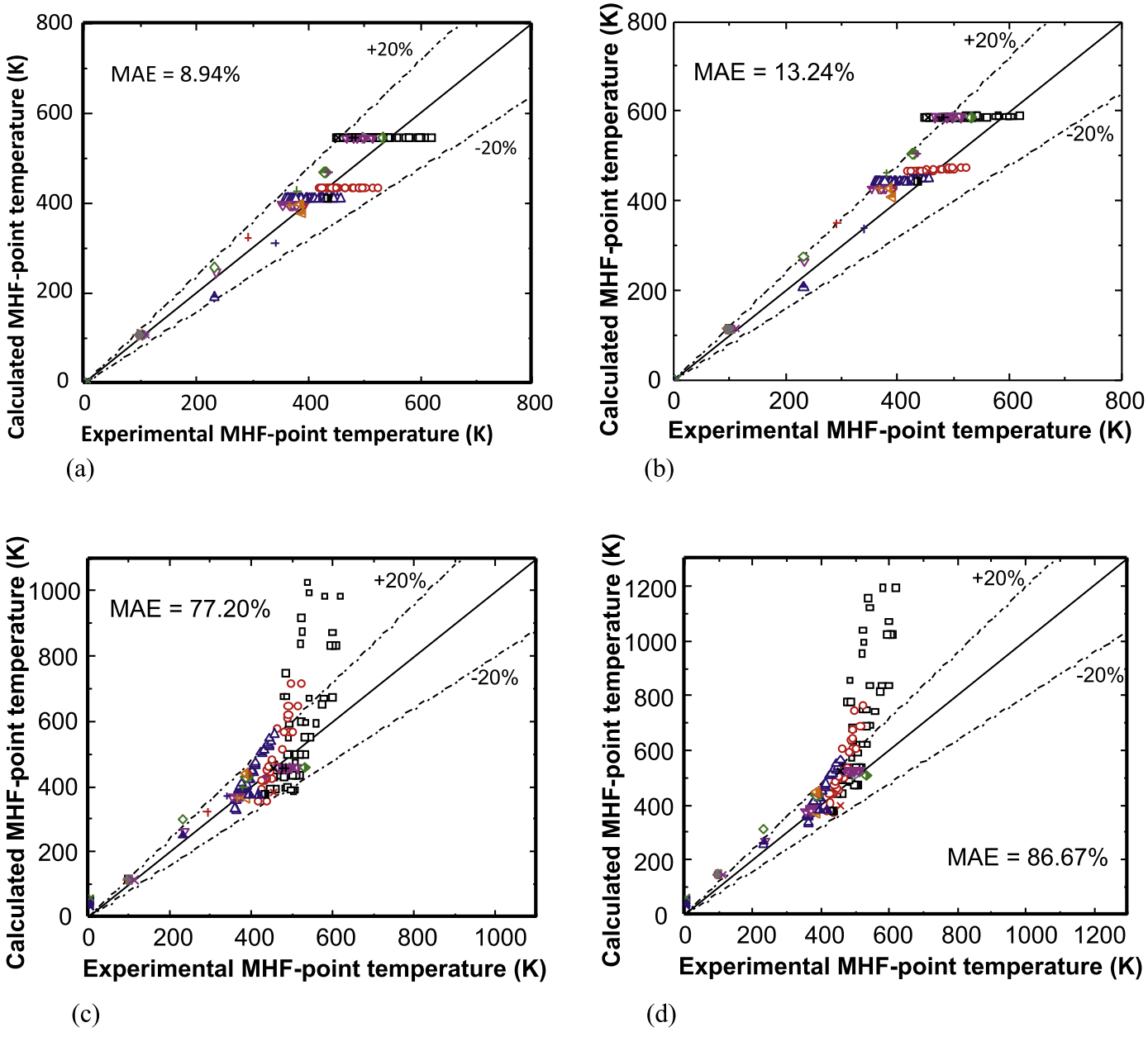

Fig. 8. Comparison of MHF-point wall temperature data with predictions of previous models by: (a) Berenson [56], (b) Siegler et al. [64], (c) Henry [57], and (d) Lienhard [65].

els show inferior predictions. Furthermore, all the models show greater discrepancies for cryogens than normal fluids.

Overall the thermodynamic models [64, 65] are able to predict the MHF-point wall temperature quite well. However, they do not provide physical insight into the underlying mechanisms. They also cannot capture the dependence of MHF-point wall temperature on system pressure, showing good results only for pressures well below critical [64]. As can also be seen in Table 2, the MHF-point wall temperature in these two formulae is only related to the liquid's critical temperature, and physical properties are not accounted for. On the other hand, both Berenson's and Henry's models (the latter is similar to the former excepting for its ability to account for wall

Table 5
Mean absolute errors of previous models in predicting pool boiling MHF-point wall temperature.

Models	Overall MAE	Overall MAE (excluding LHe)	MAE for normal fluids	MAE for cryogens	MAE for LHe	MAE for LN_2
Present model	9.35% (n = 233)	7.07% (n = 214)	6.36% (n = 151)	13.82% (n = 82)	43.10% (n = 19)	4.98% (n = 63)
Thermodynamic models						
Spiegler *et al.* [64] (1963)	8.94% (n = 233)	7.67% (n = 214)	8.08% (n =151)	10.52% (n = 82)	23.20% (n = 19)	6.70% (n = 63)
Lienhard [65] (1976)	13.24% (n = 233)	13.20% (n = 214)	12.67% (n = 151)	14.28% (n = 82)	13.68% (n = 19)	14.46% (n = 63)
Hydrodynamic models						
Berenson [56] (1961)	77.20% (n = 233)	22.08% (n = 214)	14.28% (n = 151)	193.07% (n = 82)	698.03% (n = 19)	40.79% (n = 63)
Henry [57] (1974)	86.67% (n = 223)	28.35% (n = 204)	20.24% (n = 144)	207.77% (n = 79)	712.92% (n = 19)	47.81% (n = 60)

properties) show very high error for high pressures, a weakness also identified in previous studies [32, 37]. And, despite having an MAE slightly inferior to that of Siegler *et al.* [64], the present model is both hydrodynamic and mechanistically based, and provides far better accuracy than the other two other hydrodynamic models.

For cryogenic fluids (liquid helium and liquid nitrogen), predictive accuracy for all models is inferior to that for normal fluids. This is especially the case for liquid helium when using Berenson's and Henry's hydrodynamic models, a weakness pointed out in other studies as well [28, 50].

Finally, it is important to emphasize that poor predictive capability of models is not an exclusive measure of accuracy, given the specificity of models to certain working fluids, heater sizes, and operating conditions.

4.3. Discussions on model applicability

The model developed in the current study constitutes a mechanistic approach to predicting the MHF-point wall temperature for horizontal pool boiling from an infinite flat heating surface, providing the added benefit of pinpointing a trigger event for MHF. However, future improvements may be needed to address the following issues for which the present model is not intended:

1 *Low-temperature cryogenic fluids:* In general, cryogenic fluids feature a very low boiling point, large compressibility, small density difference between the liquid and vapor phases, and small latent heat of vaporization when compared to normal fluids [112]. These unique properties (especially for liquid helium) greatly increase uncertainties in heat transfer measurements for cryogenic fluids, including the inability to accurately account for heat loss.

2 *Liquid metals:* Contrarily, liquid metals feature both very high boiling point and high thermal conductivity (the latter is generally more than an order higher than those for normal fluids) and high liquid density. With conductivity values comparable to those of the heating wall, the predicted MHF-point wall temperature must be modified to account for effects of the product $k\rho c_p$ of both the wall and liquid metal. Another unique attribute of liquid metals is the large density ratio between the liquid and vapor phases, which renders the Taylor instability easier to occur. Liquid metals, particularly alkali metals, also wet practically all solid surfaces extremely well [113], a phenomenon that plays a potentially important role in promoting liquid-solid contact in film boiling and therefore vapor film collapse, leading to higher MHF-point wall temperatures.

3 *Surface topography*: It is noteworthy that no information on surface roughness is considered in the present method. In other words, the model is intended for practical surfaces with roughness features much smaller than the vapor film thickness (~100 μm in stable film boiling for most liquids). Under such conditions, the liquid-vapor interface will remain separated from the heating surface, precluding premature collapse of film boiling. As shown in Table 1, several past studies have investigated the effects of surface topography on the MHF-point using a variety of surface modification techniques (*e.g.*, anodized [35, 44], particle-coated [36, 46, 50], grooved [27], oxidized [20, 43], nanotube-coated [47, 48]). Such artificial micro/nano structures will alter the surface roughness height, porosity and wettability considerably, which, in turn, exert a profound influence on the MHF-point; such data are therefore excluded for comparison with predictions of the present model.

4 *Subcooling:* The present model is intended only for saturated conditions and therefore does not account for condensation along the interface. Subcooling influences MHF by virtue of formation of a liquid boundary layer above the interface. Both conduction and convection effects associated with liquid motion within this layer are expected to complicate vapor film collapse at MHF.

5 *Surface size:* The present model is intended for infinite horizontal surfaces. As discussed earlier, the infinite size assumption is valid for surfaces with length scale several multiples of the critical Taylor wavelength. Although the size effect is accounted for in Klimenko's correlation [78] to relate wall temperature to heat flux, the present MHF model is developed for surface sizes much larger than the critical wavelength. Some studies have proposed a critical surface size of $2\sqrt{3}\lambda_c$ [38] or $3\sqrt{3}\lambda_c$ [41] below which the heating surface size begins to affect the MHF point.

5. Conclusions

This paper presented a new mechanistic approach to predicting wall temperature corresponding to the minimum heat flux (MHF) point for saturated pool boiling from a horizontal flat surface. The MHF condition is shown to commence once the downward forces pushing the liquid-vapor interface towards the surface overcome the upward forces lifting the interface away from the surface. This causes the wavy liquid-vapor interface to contact and wet the surface; vigorous bubble nucleation and vapor production ensue, signaling onset of the transition boiling regime. To achieve closer, two additional parameters are incorporated into the model: (a) A dimensionless multiplier addressing pressure effects, which is derived statistically form experimental data, and (b) a previous relation for film boiling heat transfer coefficient, which is used to determine the wall temperature. Key conclusions from the study are as follows:

(1) The new mechanistic approach shows very good accuracy in predicting the MHF-point wall temperature for many liquids and a broad range of pressures, evidenced by an overall MAE of 9.35%.

(2) While previous thermodynamic models of MHF-point wall temperature show fairly good agreement with experimental data, they do not capture the trigger mechanism for MHF. The hydrodynamic models yield high errors for high-pressure conditions.

(3) Application of the new model is carefully addressed, which points to future research needs to explore effects of liquid subcooling, surface size and topography, and unique properties of liquid metals and cryogenic fluids.

Declaration of Competing Interest

None. The authors declare that they have no known competing financial interests or personal relationships that could have appeared to influence the work reported in this paper.

Acknowledgments

Financial support from National Key Research and Development Program of China (grant no. 2017YFA0700300), National Natural Science Foundation of China (grant no. 51961135105, 91641117), Open subject of the State Key Laboratory of Engines (Tianjin University) (grant no. K2018-04) and China Scholarship Council (grant no. 201806060070) is gratefully acknowledged.

Supplementary materials

Supplementary material associated with this article can be found, in the online version, at doi:10.1016/j.ijheatmasstransfer.2020.119854.

References

[1] I. Mudawar, Recent advances in high-flux, two-phase thermal management, J. Therm. Sci. Eng. Appl. 5 (2013) 021012.
[2] H. Zhang, I. Mudawar, M.M. Hasan, Experimental and theoretical study of orientation effects on flow boiling CHF, Int. J. Heat Mass Transfer 45 (2002) 4463–4477.
[3] C. Konishi, I. Mudawar, Review of flow boiling and critical heat flux in microgravity, Int. J. Heat Mass Transfer 80 (2015) 469–493.
[4] T.J. LaClair, I. Mudawar, Thermal transients in a capillary evaporator prior to the initiation of boiling, Int. J. Heat Mass Transfer 43 (2000) 3937–3952.
[5] I. Mudawar, T.M. Anderson, Parametric investigation into the effects of pressure, subcooling, surface augmentation and choice of coolant on pool boiling in the design of cooling systems for high-power-density electronic chips, J. Electron. Packag. 112 (1990) 375–382.
[6] I. Mudawar, R.A. Houpt, Mass and momentum transport in smooth falling liquid films laminarized at relatively high Reynolds numbers, Int. J. Heat Mass Transfer 36 (1993) 3437–3448.
[7] C.O. Gersey, I. Mudawar, Effects of heater length and orientation on the trigger mechanism for near-saturated flow boiling critical heat flux—I. Photographic study and statistical characterization of the near-wall interfacial features, Int. J. Heat Mass Transfer 38 (1995) 629–641.
[8] C.O. Gersey, I. Mudawar, Effects of heater length and orientation on the trigger mechanism for near-saturated flow boiling critical heat flux—II. Critical heat flux model, Int. J. Heat Mass Transfer 38 (1995) 643–654.
[9] S. Mukherjee, I. Mudawar, Pumpless loop for narrow channel and micro-channel boiling, J. Electron. Packag. 125 (2003) 431–441.
[10] M.E. Johns, I. Mudawar, An ultra-high power two-phase jet-impingement avionic clamshell module, J. Electron. Packag. 118 (1996) 264–270.
[11] W.P. Klinzing, J.C. Rozzi, I. Mudawar, Film and transition boiling correlations for quenching of hot surfaces with water sprays, J. Heat Treating 9 (1992) 91–103.
[12] M.K. Sung, I. Mudawar, Single-phase and two-phase heat transfer characteristics of low temperature hybrid micro-channel/micro-jet impingement cooling module, Int. J. Heat Mass Transfer 51 (2008) 3882–3895.
[13] S.-M. Kim, I. Mudawar, Universal approach to predicting saturated flow boiling heat transfer in mini/micro-channels–Part I. Dryout incipience quality, Int. J. Heat Mass Transfer 64 (2013) 1226–1238.
[14] S.-M. Kim, I. Mudawar, Review of databases and predictive methods for pressure drop in adiabatic, condensing and boiling mini/micro-channel flows, Int. J. Heat Mass Transfer 77 (2014) 74–97.
[15] H. Lee, C.R. Kharangate, N. Mascarenhas, I. Park, I. Mudawar, Experimental and computational investigation of vertical downflow condensation, Int. J. Heat Mass Transfer 85 (2015) 865–879.
[16] S.-M. Kim, I. Mudawar, Theoretical model for annular flow condensation in rectangular micro-channels, Int. J. Heat Mass Transfer 55 (2012) 958–970.
[17] C.R. Kharangate, I. Mudawar, Review of computational studies on boiling and condensation, Int. J. Heat Mass Transfer 108 (2017) 1164–1196.
[18] G. Liang, I. Mudawar, Pool boiling critical heat flux (CHF)—Part 1: Review of mechanisms, models, and correlations, Int. J. Heat Mass Transfer 117 (2018) 1352–1367.
[19] G. Liang, I. Mudawar, Pool boiling critical heat flux (CHF)—Part 2: Assessment of models and correlations, Int. J. Heat Mass Transfer 117 (2018) 1368–1383.
[20] P.J. Berenson, Experiments on pool-boiling heat transfer, Int. J. Heat Mass Transfer 5 (1962) 985–999.
[21] E.R. Hosler, W.J. W., Film boiling on a horizontal plate, ARS J 32 (1962) 553–558.
[22] R.D. Cummings, J.L. Smith, in: Boiling heat transfer to liquid helium, Pergamon Press, Oxford, 1966, pp. 85–95.
[23] A. Padilla, Film boiling of potassium on a horizontal plate, University of Michigan, Michigan, USA, 1966.
[24] J.A. Clark, E.W. Lewis, H. Merte Jr, Boiling of liquid nitrogen in reduced gravity fields with subcooling, Heat Transfer Lab., Dept. Mech. Engng, Univ. of Michigan, Michigan, 1967.
[25] R.C. Kesselring, P.H. Rosche, S.G. Bankoff, Transition and film boiling from horizontal strips, AIChE J. 13 (1967) 669–675.
[26] A.P. Butler, G.B. James, B.J. Maddock, W.T. Norris, Improved pool boiling heat transfer to helium from treated surfaces and its application to superconducting magnets, Int. J. Heat Mass Transfer 13 (1970) 105–115.
[27] F. Tachibana, S. Enya, Heat transfer problems in quenching, Bull. JSME 16 (1973) 100–109.
[28] J.L. Swanson, H.F. Bowman, J.L. Smith Jr, Transient surface temperature behavior in the film boiling region, Tran. Can. Soc. Mech. Eng. 3 (1975) 131–140.
[29] V.I. Deev, V.E. Keilin, I.A. Kovalev, A.K. Kondratenko, V.I. Petrovichev, Nucleate and film pool boiling heat transfer to saturated liquid helium, Cryogenics 17 (1977) 557–562.
[30] W. Peyayopanakul, J.W. Westwater, Evaluation of the unsteady-state quenching method for determining boiling curves, Int. J. Heat Mass Transfer 21 (1978) 1437–1445.
[31] E.A. Ibrahim, R.W. Boom, G.E. McIntosh, Heat transfer to subcooled liquid helium, in: Adv. Cryogen. Eng., Springer, 1978, pp. 333–339.
[32] S.C. Yao, R.E. Henry, An investigation of the minimum film boiling temperature on horizontal surfaces, J. Heat Transfer 100 (1978) 260–267.
[33] H. Kobayashi, K. Yasukōchi, Maximum and minimum heat flux and temperature fluctuation in film-boiling states in superfluid Helium, in: Adv. Cryogen. Eng., Springer, 1980, pp. 372–377.
[34] M.W. Scheiwe, U. Hartmann, Heat transfer from warm plates of cryobiologic interest to liquid nitrogen, in: Ninth Int. Cryogenic Eng. Conf., Elsevier, Kobe, 1982, pp. 81–84.
[35] D.S. Dhuga, R.H.S. Winterton, Measurement of surface contact in transition boiling, Int. J. Heat Mass Transfer 28 (1985) 1869–1880.
[36] D.S. Jung, J.E.S. Venart, A.C.M. Sousa, Effects of enhanced surfaces and surface orientation on nucleate and film boiling heat transfer in R-11, Int. J. Heat Mass Transfer 30 (1987) 2627–2639.
[37] M. Shoji, H. Nagano, Mininum heat flux of saturated pool boiling on a horizontal heated surface, Tran. Jap. Soc. Mech. Eng, Series B 52 (1987) 2431–2436.
[38] M. Shoji, A. Okamoto, Y. Kaneko, M. Kawada, Effects of size and end conditions of a heated surface upon minimum film boiling, JSME Int. J. 30 (1987) 1587–1594.
[39] J.M. Ramilison, J.H. Lienhard, Transition boiling heat transfer and the film transition regime, J. Heat Transfer 109 (1987) 746–752.
[40] S. Nishio, G.R. Chandratilleke, Steady-state pool boiling heat transfer to saturated liquid helium at atmospheric pressure, JSME Int. J. 32 (1989) 639–645.
[41] A. Abbassi, A.A.A. Rajabi, R.H.S. Winterton, Effect of confined geometry on pool boiling at high temperature, Exp. Therm. Fluid Sci. 2 (1989) 127–133.
[42] J.W. Westwater, J.C. Zinn, K.J. Brodbeck, Correlation of pool boiling curves for the homogeous group: Freons, J. Heat Transfer 11 (1989) 204–206.
[43] M. Shoji, L.C. Witte, S. Yokoya, M. Ohshima, Liquid-solid contact and effects of surface roughness and wettability in film and transition boiling on a horizontal large surface, in: Proc. Nineth Int. Heat Transfer Conf., Begel House Inc., Jerusalem, 1990, pp. 135–141.
[44] I. Rajab, R.H.S. Winterton, The two transition boiling curves and solid-liquid contact on a horizontal surface, Int. J Heat Fluid Flow 11 (1990) 149–153.
[45] J.Y. Chang, S.M. You, A. Haji Sheikh, Film boiling incipience at the departure from natural convection on flat, smooth surfaces, J. Heat Transfer 120 (1998) 402–409.
[46] Y. Takata, S. Hidaka, J.M. Cao, T. Nakamura, H. Yamamoto, M. Masuda, T. Ito, Effect of surface wettability on boiling and evaporation, Energy 30 (2005) 209–220.
[47] H.S. Ahn, V. Sathyamurthi, D. Banerjee, Pool boiling experiments on a nano-structured surface, IEEE Trans. Compon. Packag. Technol. 32 (2009) 156–165.
[48] V. Sathyamurthi, H.S. Ahn, D. Banerjee, S.C. Lau, Subcooled pool boiling experiments on horizontal heaters coated with carbon nanotubes, J. Heat Transfer 131 (2009) 071501.
[49] C. Zhao, M.Q. Gong, L. Ding, X. Zou, G.F. Chen, J.F. Wu, An experimental investigation on the entire pool boiling curve of R14 under 0.1 MPa pressure, Int. J. Refrig. 41 (2014) 164–170.
[50] R. Li, Z. Huang, X. Wu, P. Yan, X. Dai, Cryogenic quenching of rock using liquid nitrogen as a coolant: Investigation of surface effects, Int. J. Heat Mass Transfer 119 (2018) 446–459.
[51] K.J. Baumeister, F.F. Simon, Leidenfrost temperature—Its correlation for liquid metals, cryogens, hydrocarbons, and water, J. Heat Transfer 95 (1973) 166–173.
[52] N. Shigefumi, Prediction technique for minimum-heat-flux (MHF)-point condition of saturated pool boiling, Int. J. Heat Mass Transfer 30 (1987) 2045–2057.
[53] V.V. Klimenko, S.Y. Snytin, Film boiling crisis on a submerged heating surface, Exp. Therm. Fluid Sci. 3 (1990) 467–479.
[54] E.K. Kalinin, Berlin II, V.V. Kostyuk, E.M. Nosova, Heat transfer in transition boiling of cryogenic liquids, in: Adv. Cryogen. Eng., Springer, 1960, pp. 273–277.
[55] N. Zuber, Hydrodynamic aspects of boiling heat transfer, University of California, Los Angeles, USA, 1959.

[56] P.J. Berenson, Film boiling heat transfer from a horizontal surface, J. Heat Transfer 83 (1961) 351–358.
[57] R.E. Henry, A correlation for the minimum film boiling temperature, AIChE Sympos. Ser. 138 (1974) 81–90.
[58] F.S. Gunnerson, A.W. Cronenberg, On the minimum film boiling conditions for spherical geometries, J. Heat Transfer 102 (1980) 335–341.
[59] F.S. Gunnerson, A.W. Cronenberg, Film boiling and vapor explosion phenomena, Nucl. Technol. 49 (1980) 380–391.
[60] V.K. Dhir, Discussion: "On the minimum film boiling conditions for spherical geometries" (Gunnerson, FS, and Cronenberg, AW, 1980, ASME J. Heat Transfer, 102, pp. 335-341), J. Heat Transfer 102 (1980). 790–790.
[61] X. Ma, P. Cheng, Dry spot dynamics and wet area fractions in pool boiling on micro-pillar and micro-cavity hydrophilic heaters: A 3D lattice Boltzmann phase-change study, Int. J. Heat Mass Transfer 141 (2019) 407–418.
[62] X. Ma, P. Cheng, 3D simulations of pool boiling above smooth horizontal heated surfaces by a phase-change lattice Boltzmann method, Int. J. Heat Mass Transfer 131 (2019) 1095–1108.
[63] S. Gong, P. Cheng, Direct numerical simulations of pool boiling curves including heater's thermal responses and the effect of vapor phase's thermal conductivity, Int. Comm. Heat Mass Transfer 87 (2017) 61–71.
[64] P. Spiegler, J. Hopenfeld, M. Silberberg, C.F. Bumpus Jr, A. Norman, Onset of stable film boiling and the foam limit, Int. J. Heat Mass Transfer 6 (1963) 987–989.
[65] J.H. Lienhard, Correlation for the limiting liquid superheat, Chem. Eng. Sci. 31 (1976) 847–849.
[66] F.S. Gunnerson, A.W. Cronenberg, On the thermodynamic superheat limit for liquid metals and its relation to the Leidenfrost temperature, J. Heat Transfer 100 (1978) 734–737.
[67] A. Segev, S.G. Bankoff, The role of adsorption in determining the minimum film boiling temperature, Int. J. Heat Mass Transfer 23 (1980) 637–642.
[68] M. Poniewski, Dissipative model of film boiling crisis, Int. J. Heat Mass Transfer 30 (1987) 1847–1857.
[69] S. Olek, Y. Zvirin, E. Elias, The relation between the rewetting temperature and the liquid-solid contact angle, Int. J. Heat Mass Transfer 31 (1988) 898–902.
[70] A.W. Adamson, Potential distortion model for contact angle and spreading. II. temperature dependent effects, J. Colloid Interface Sci. 44 (1973) 273–281.
[71] D. Schroeder-Richter, G. Bartsch, The Leidenfrost phenomenon caused by a thermo-mechanical effect of transition boiling: a revisited problem of non-equilibrium thermodynamics, ASME, New York, New York, 1990.
[72] C.T. Avedisian, The homogeneous nucleation limits of liquids, J. Phys. Chem. Ref. Data 14 (1985) 695–729.
[73] V.P. Carey, Liquid vapor phase change phenomena: An introduction to the thermophysics of vaporization and condensation processes in heat transfer equipment, Hemisphere, New York, 1992.
[74] V. Gerweck, G. Yadigaroglu, A local equation of state for a fluid in the presence of a wall and its application to rewetting, Int. J. Heat Mass Transfer 35 (1992) 1823–1832.
[75] J.D. Bernardin, I. Mudawar, A cavity activation and bubble growth model of the Leidenfrost point, J. Heat Transfer 124 (2002) 864–874.
[76] E. Aursand, S.H. Davis, T. Ytrehus, Thermocapillary instability as a mechanism for film boiling collapse, J. Fluid Mech 852 (2018) 283–312.
[77] S.S. Kutateladze, Heat transfer in condensation and boiling, AEC-tr-3770 (1959).
[78] V.G. Morozov, An experimental investigation of the cessation of film boiling of a liquid on a submerged heating surface, Int. Chem. Eng. 3 (1963) 48–51.
[79] E. Ruckenstein, Film boiling on a horizontal surface, Int. J. Heat Mass Transfer 10 (1967) 911–919.
[80] J.H. Lienhard, V.K. Dhir, On the prediction of the minimum pool boiling heat flux, J. Heat Transfer 102 (1980) 457–460.
[81] I. Sher, R. Harari, R. Reshef, E. Sher, Film boiling collapse in solid spheres immersed in a sub-cooled liquid, Appl. Therm. Eng. 36 (2012) 219–226.
[82] B.J. Kim, J.H. Lee, K.D. Kim, Rayleigh–Taylor instability for thin viscous gas films: application to critical heat flux and minimum film boiling, Int. J. Heat Mass Transfer 80 (2015) 150–158.
[83] L.D. Clements, C.P. Colver, Natural convection film boiling heat transfer, Ind. Eng. Chem. 62 (1970) 26–46.
[84] M. Koc, J. Culp, T. Altan, Prediction of residual stresses in quenched aluminum blocks and their reduction through cold working processes, J. Mater. Process. Technol. 174 (2006) 342–354.
[85] S. Nishio, M. Uemura, K. Sakaguchi, Film boiling heat transfer and minimum-heat-flux (MHF)-point condition in subcooled pool boiling: heat transfer, power, combustion, thermophysical properties, JSME Int. J. 30 (1987) 1274–1281.
[86] V.V. Klimenko, Film boiling on a horizontal plate—new correlation, Int. J. Heat Mass Transfer 24 (1981) 69–79.
[87] R. Sadeghi, M.S. Shadloo, Three-dimensional numerical investigation of film boiling by the Lattice Boltzmann method, Numer. Heat Transfer, Part A. App. 71 (2017) 560–574.
[88] J.M. Ramilison, J.H. Lienhard, Transition boiling heat transfer and the film transition regime, J. Heat Transfer 109 (1987) 746–752.
[89] V.V. Klimenko, A.G. Shelepen, Film boiling on a horizontal plate—a supplementary communication, Int. J. Heat Mass Transfer 25 (1982) 1611–1613.
[90] F.M. Verplaetsen, J.A. Berghmans, Film boiling of an electrically insulating fluid in the presence of an electric field, Heat Mass Transfer 35 (1999) 235–241.
[91] A. Begmohammadi, M.H. Rahimian, M. Farhadzadeh, M.A. Hatani, Numerical simulation of single-and multi-mode film boiling using lattice Boltzmann method, Comp. Math. Appl. 71 (2016) 1861–1874.
[92] S.A. Hosseini, R. Kouhikamali, A numerical investigation of various phase change models on simulation of saturated film boiling heat transfer, Heat Transfer Asian Res 48 (2019) 2577–2595.
[93] Y.-Y. Tsui, S.-W. Lin, Three-dimensional modeling of fluid dynamics and heat transfer for two-fluid or phase change flows, Int. J. Heat Mass Transfer 93 (2016) 337–348.
[94] M.W. Akhtar, S.J. Kleis, Boiling flow simulations on adaptive octree grids, Int. J. Multiph. Flow 53 (2013) 88–99.
[95] S.W.J. Welch, T. Rachidi, Numerical computation of film boiling including conjugate heat transfer Numer, Heat Transfer, Part B. Fund. 42 (2002) 35–53.
[96] M. Ahammad, Y. Liu, T. Olewski, L.N. Véchot, M.S. Mannan, Application of computational fluid dynamics in simulating film boiling of cryogens, Ind. Eng. Chem. Res. 55 (2016) 7548–7557.
[97] Y.P. Chang, Wave theory of heat transfer in film boiling, J. Heat Transfer 81 (1959) 1–8.
[98] T.D. Hamill, K.J. Baumeister, Film boiling heat transfer from a horizontal surface as an optimal boundary value process, in: Proc. 3rd Int. Heat Trans. Conf., Begel House Inc., 1966, pp. 59–64.
[99] T.H.K. Frederking, Y. Wu, B.W. Clement, Effects of interfacial instability on film boiling of saturated liquid helium I above a horizontal surface, AIChE J. 12 (1966) 238–244.
[100] Y.J. Lao, R.E. Barry, R.E. Balzhiser, A study of film boiling on a horizontal plate, in: Proc. 4th Int. Heal Transfer Conf., Begel House Inc., Paris, Versailles, 1970 B3.10.
[101] T. Hiroaki, On the stability of vapor film in pool film boiling, Int. J. Heat Mass Transfer 31 (1988) 129–134.
[102] V.K. Dhir, Numerical simulations of pool-boiling heat transfer, AIChE J. 47 (2001) 813–834.
[103] P. Zhang, M. Murakami, Experimental investigation of the film boiling heat transfer in He II: Heat transfer coefficient, Cryogenics 45 (2005) 77–83.
[104] H.J. Sauer, K.M. Ragsdell, Film pool boiling of nitrogen from flat surfaces, in: Adv. Cryogen. Eng., Springer, 1971, pp. 412–415.
[105] L.M. Milne-Thompson, Theoretical hydrodynamics, (Forth ed.), Macmillan, New York, 1960.
[106] NIST, Standard Reference Database-REFPROP Version 8.0, National Institute of Standard and Technology, Boulder, Colorado, 2007.
[107] S. Nishio, Study on the minimum heat flux point for boiling heat transfer on a horizontal flat plate (effects of transients and thermal conductance of surface), Heat Transfer-Jap. Res. 15 (1986) 15–33.
[108] K. Nishikawa, S. Hasegdwa, N. Kitayama, K. Sakamoto, The effects of heating surface conditions on the transition boiling, Technol. Report.u Kyushu Unit. 27 (1966) 399–404.
[109] K. Nishikawa, S. Hasegawa, T. Iwabuchi, Y. Miyabara, Characteristics of transition boiling on the horizontal plate, Technol. Reports Kyushu Univ. 38 (1965) 306–311.
[110] V.P. Skrinov, Metastable liquids, Wilev, New York, 1974.
[111] F.P. Incropera, A.S. Lavine, T.L. Bergman, D.P. DeWitt, Fundamentals of heat and mass transfer, Wiley, New York, 2007.
[112] J. Ishimoto, K. Kamijo, Numerical study of cavitating flow characteristics of liquid helium in a pipe, Int. J. Heat Mass Transfer 47 (2004) 149–163.
[113] W.M. Rohsenow, Boiling, Annu. Rev. Fluid Mech. 3 (1971) 211–236.